CHAPTER 59

Pillar Design to Prevent Collapse of Room-and-Pillar Mines

R. Karl Zipf, Jr.*

59.1 INTRODUCTION

Room-and-pillar mining accounts for a significant portion of the total mineral production in the United States. As shown in Table 59.1, well in excess of $6 billion worth of mineral commodities is produced each year by this method. A substantial portion ($3.55 billion) of coal production still comes from room-and-pillar mining. Metallic minerals valued at about $1 billion, plus nonmetallic minerals valued well in excess of $1 billion, are also produced via room-and-pillar mining. A significant ($600 million) and growing portion of stone and aggregate production uses room-and-pillar mining. In addition, many other mineral commodities not noted in this table such as talc, iron, and copper are or have been produced in the United States using the room-and-pillar technique.

Comparing current data with 1973 data compiled by Bullock (1982) shows that production by room-and-pillar method has declined in some commodities and grown in others. For example, coal production by room-and-pillar method has declined from 90% of coal production then to 20% of the total today. However, since 1973, total coal production has almost tripled so that in terms of tons, room-and-pillar coal production has declined only from about 290 to 200 million tons today, which is still a very significant production amount. Prior to 1973, the room-and-pillar mining technique accounted for 60% of noncoal mineral production or about 80 million tons of material. Today, the method probably accounts for no more than about 20% of total noncoal production; however, as shown in Table 59.1, the tonnage and value is very significant. Large increases in noncoal mineral production using the room-and-pillar method have occurred in soda ash, potash, salt, and most recently in stone and aggregate.

One important parameter in the engineering of room-and-pillar mines is the pillar size, which coupled with the room width determines the achievable extraction percentage. Several opposing factors influence the choice of pillar size. Sizing pillars too large leaves valuable resources in the earth and risks poorer mining economics and waste of scarce mineral deposits. Sizing a pillar too small risks pillar failure and potential surface subsidence. Pillars that are too small can lead to a large-scale catastrophic collapse called a cascading pillar failure, which carries severe economic and health and safety risks (Zipf 1996 and Zipf and Swanson 1999). As shown in Table 59.1, with mineral production valued at over $6 billion coming from room-and-pillar mines, changing the extraction percentage by just 1% translates into over $60 million per year in resource conservation or mining revenue gains. Better understanding of pillar mechanics will therefore have significant impact on the economics of mines using the room-and-pillar method.

The objective of this paper is to present a design methodology aimed at eliminating the risk of large-scale pillar collapse in room-and-pillar mines. The design methodology involves evaluation of Salamon's local mine stiffness stability criterion. This section first summarizes traditional strength-based pillar design methods applicable to coal or hard-rock mines. Several examples of large-scale pillar collapse are reviewed, and the mechanics of these failures is presented. To decrease the risk of pillar collapse, three alternative design approaches are given—the containment approach, the prevention approach, and the full extraction approach. Finally, practical methods are presented to evaluate the local mine stiffness stability criterion and use results in practical room-and-pillar mine layout.

59.2 TRADITIONAL STRENGTH-BASED PILLAR DESIGN METHODS

Room-and-pillar mines may cover a small area several hundred feet square and contain just a few pillars as in a small zinc deposit. Alternatively, they may cover many square miles as is typical with coal, trona, or limestone mines. Large arrays of pillars are typically grouped into panels, which are in turn surrounded by barrier pillars. The small pillars within a panel are sometimes called panel pillars. Figure 59.1 shows typical layouts for coal, limestone, and lead room-and-pillar mines. In developing these layouts, the mining engineer must develop appropriate dimensions for the room spans, panel pillar widths, panel sizes and finally barrier pillar widths. In addition to strength considerations, developing these dimensions requires evaluation of the consequences of pillar failure, which could happen anywhere in the layout at any time.

Traditional strength-based pillar design first requires an estimate of pillar stress and then an estimate of pillar strength. The safety factor for the pillar is then evaluated as pillar strength over pillar stress. An acceptable safety factor depends on the tolerable risk of failure. A safety factor of 2 is typical for pillars in main development headings or panels during advance mining. Safety factors of 1.1 to 1.3 are typical for panel pillars after retreat mining. Safety factors much less than one are possible within panels where pillar failure is the intent.

59.2.1 Pillar Stress

As summarized by Farmer (1992), traditional pillar design for room-and-pillar mining begins by estimating the in situ vertical stress as

$$\sigma_z = \lambda z \qquad (59.1)$$

where λ is the unit weight of rock and z is depth to the mining horizon. The tributary area method then provides a first-order estimate of the average pillar stress. For the square room-and-pillar system shown in Figure 59.2, the average pillar stress is:

* NIOSH, Spokane Research Laboratory, Spokane, WA.

TABLE 59.1 Value and production by room-and-pillar mining in the United States

Mineral commodity	Totabl U.S. production (tons)	Approximate % by room-and-pillar	Room-and-pillar production (tons)	Value of room-and-pillar production	Typical extraction %
Coal (1)	1,014,000,000	20	202,000,000	$3,550 million	60
Lead (2)	493,000	90	444,000	$432 million	75
Zinc (2)	722,000	60	433,000	$491 million	75
Soda Ash (2)	10,100,000	80	8,000,000	$664 million	65
Potash (2)	1,300,000	100	1,300,000	$320 million	50
Salt (2)	40,800,000	60	32,000,000	$592 million	50
Gypsum (2)	19,000,000	50	9,000,000	$66 million	75
Stone and Agregate (3)	1,200,000,000	10	120,000,000	$600 million	75

(1) Coal Data 1999—National Mining Association.
(2) USGS Mineral Industry Surveys, 1998.
(3) The Aggregate Handbook—National Stone Association—1996.

$$\sigma_{pa} = \sigma_z\left(\frac{W_p + W_o}{W_p}\right)^2 \tag{59.2}$$

where W_p is the pillar width and W_o is the opening width. For rectangular or irregular-shaped pillars, the average pillar stress is found using the extraction ratio as:

$$\sigma_{pa} = \sigma_z\left(\frac{1}{1-R}\right) \tag{59.3}$$

where R is the extraction ratio.

R is found as:

$$R = \frac{A_M}{A_T} = \frac{A_T - A_P}{A_T} \tag{59.4}$$

where A_T is the total area of the orebody, A_M is the area extracted and A_P is the pillar area.

The tributary area approach assumes that the mined area is extensive and that all the pillars have the same dimensions. It also ignores the deformation properties of the surrounding rock mass relative to the pillar rock. In general, pillars at the center of a panel have a higher stress than pillars at the edge of a panel. Coates (1981) solved part of this problem by developing the following relation for average pillar stress that accounts for the width and number of pillars across a panel and the relative mechanical properties of the pillar and rock mass:

$$\sigma_{pa} = \sigma_z\left\{\frac{\left[2R - K_0\frac{H}{L}\frac{(1-2\upsilon_{rm})}{(1-\upsilon_{rm})} - \frac{\upsilon_p}{(1-\upsilon_p)}K_0\frac{H}{L}\frac{E_{rm}}{E_p}\right]}{\frac{H}{L}\frac{E_{rm}}{E_p} + 2(1-R)\left(1+\frac{1}{N}\right) + 2\frac{RB}{L}\frac{(1-2\upsilon_{rm})}{(1-\upsilon_p)}}\right\} \tag{59.5}$$

where H is the mining height, L is the lateral extent of the mined area, B is the individual opening width, N is the number of pillars across the panel, K_0 is the ratio of horizontal to vertical stress, E and υ are elastic constants, and subscripts rm and p indicate the rock mass and pillar, respectively. While this equation is based on two-dimensional elasticity theory and therefore only applies to long, narrow rib pillars, it illustrates the behavior of average pillar stress. As the E_{rm}/E_p ratio rises, the average pillar stress decreases due to the bridging effect of the stiff rock mass. Similarly as the panel width L decreases and the H/L ratio increases, average pillar stress decreases.

Similar to tributary area method, Coates' (1981) solution only gives average pillar stress for all panel pillars and does not give changes in pillar stress across the panel. Two-dimensional boundary-element-method programs such as Examine^{TAB} (2000) or quasi-three-dimensional BEM programs such as MULSIM/NL (Zipf, 1992a,b) and LAMODEL (Heasley 1997 and Heasley 1998) are needed to calculate changing pillar stresses across a panel or within an individual pillar. Figure 59.3 shows the changing stresses across a panel and within pillars using a BEM program.

59.2.2 Pillar Strength

Over the past several decades, a large amount of rock mechanics literature has addressed pillar strength, both in coal and metal/nonmetal mines (Obert and Duvall 1967; Hoek and Brown 1980; Bieniawski 1992; Brady and Brown 1993). Much of this work is empirical and has addressed two issues—the size effect whereby rock strength diminishes as specimen size increases and the shape effect whereby rock strength increases as width-to-height ratio increases. Using energy considerations, Farmer (1985) developed theoretical expressions relating strength to size. When failure occurs in a brittle manner, as it does in most rocks, strain energy within the specimen transforms to fracture surface energy, which is a constant for a particular rock. Based on energy conservation:

$$SED \times V = FE \times A \tag{59.6}$$

where SED is the strain-energy-density of the rock, V is the rock volume, FE is the fracture-surface-energy, which is a material constant, and A is the fracture surface area.

Rearranging gives:

$$SED \times \frac{V}{A} = SED \times L = FE = \text{constant} \tag{59.7}$$

where L is a characteristic dimension or length of the rock specimen.

Assuming that laboratory-scale failure is mechanistically similar to full-scale pillar failure, then

$$SED_S \times L_S = SED_P \times L_P \tag{59.8}$$

where the subscripts S and P indicate laboratory-scale specimen and full-scale pillar, respectively. Since strain-energy-density at failure is proportional to the square of stress at failure,

$$\sigma_S^2 \times L_S = \sigma_P^2 \times L_P \tag{59.9}$$

or

$$\frac{\sigma_P}{\sigma_S} = \left(\frac{L_S}{L_P}\right)^{1/2} = \left(\frac{V_S}{V_P}\right)^{1/6} = \left(\frac{V_S}{V_P}\right)^{0.17} \tag{59.10}$$

where σ_S and σ_P are strength of the laboratory specimen and full-scale pillar, respectively and V is volume, which is proportional to L^3. This theoretical relationship accounts for the size effect in

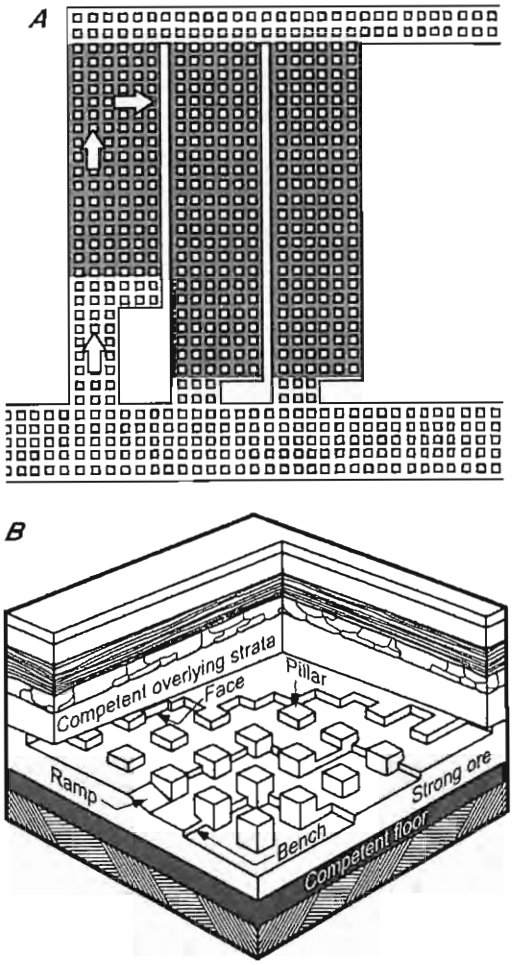

FIGURE 59.1 A: Typical room-and-pillar layout for coal mine with pillar extraction on retreat (Farmer 1992); B: Typical room-and-pillar layout for metal/nonmetal mine (Dravo 1974)

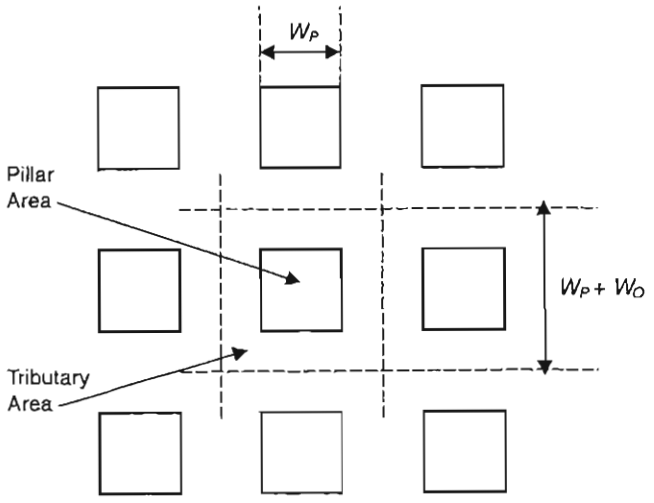

FIGURE 59.2 Plan view of room-and-pillar mine with dimensions for simple analysis

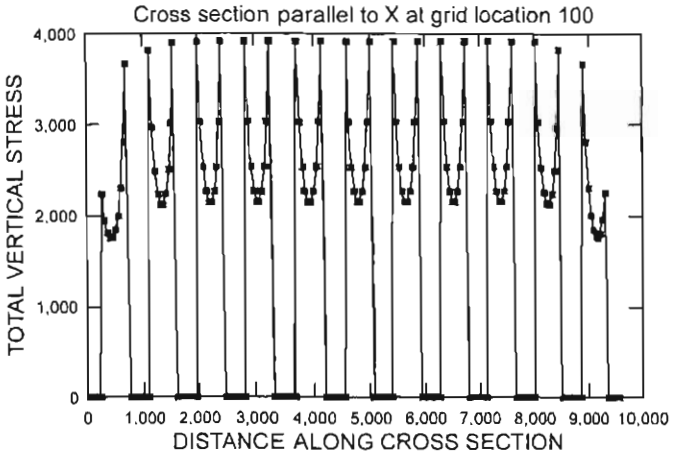

FIGURE 59.3 Pillar stresses across a panel and within pillars determined with the boundary element method probram MULSIM/NL

observed rock strength. The following empirical strength formula proposed by Hardy and Agapito (1977) for oil shale pillars follows this general theoretical form and provides some experimental confirmation.

$$\frac{\sigma_p}{\sigma_S} = \left(\frac{V_S}{V_p}\right)^{0.118}\left[\frac{W_p}{H_p}\frac{H_S}{W_S}\right]^{0.833} \qquad (59.11)$$

where W and H are pillar and specimen width respectively. This empirical model also includes an additional term for pillar shape.

Classic empirical pillar strength formulas usually follow one of two general forms.

$$\sigma_p = \sigma_{S'}\left(a + b\frac{W}{H}\right) \qquad (59.12)$$

$$\sigma_p = K\frac{W^{\alpha}}{H^{\beta}} \qquad (59.13)$$

Pillar strength formulas by Obert and Duvall (1967) and Bieniawski (1968a) follow the first form, whereas formulas by Salamon and Munro (1967) and Holland (1964) follow the second. In these forms, size effect is accounted for directly via the unit pillar strength $\sigma_{S'}$ or the rock constant K. $\sigma_{S'}$ is the strength of a cubical pillar ($W/H = 1$) at or above the critical size, and K is a constant characteristic of the pillar rock. The constants a, b, α and β in these equations account for the shape factor and show reasonable agreement as shown Table 59.2.

Several methods exist for estimating $\sigma_{S'}$ or K in equations 12 or 13, which is the strength of a cubical pillar ($W/H = 1$) at or above the critical size, where critical size is that size beyond which the rock mass strength remains relatively constant. For coal pillars, the critical size is widely recognized as about 0.9 meter or 36 inches. For U.S coal mines, the recommended strength value for a cube of coal this size is $\sigma_{S'} = 6.2$ MPa or 900 psi (Mark 1997b). This unit strength for a full-scale cube of coal can then be adjusted for shape effect using the recent Mark-Bieniawski relation (Mark 1999):

$$\sigma_p = \sigma_{S'}\left(0.64 + 0.54\frac{W}{H} - 0.18\frac{W^2}{HL}\right) \qquad (59.14)$$

which reduces to the original Bieniawski relation when pillar width W equals pillar length L.

TABLE 59.2 Values for constants in empirical pillar strength formulas

Source	a	b	α	β	Comments
Bunting (1911)	0.7	0.3	—	—	Pennsylvania anthracite
Obert and Duvall (1967)	0.78	0.22	—	—	Laboratory rock and coal
Bieniawski (1968a)	0.64	0.36	—	—	South Africa coal
Skelly, Wolgamott and Wang (1977)	0.78	0.22	—	—	West Virginia coal
Greenwald, Howarth and Hartman (1939)	—	—	0.5	0.83	Pittsburgh seam mines
Holland (1964)	—	—	0.5	1	U.S. coal mines
Salamon and Munro (1967)	—	—	0.46	0.66	S.A. coal mines
Hardy and Agapito (1977)	—	—	0.60	0.95	U.S. oil shale mines

If laboratory-scale strength data (σ_S) is available, the full-scale strength of a cube of rock mass ($\sigma_{S'}$) can be found from equation 10 as:

$$\sigma_{S'} = \sigma_S\left(\frac{V_S}{V_{S'}}\right)^{0.17} \quad (59.15)$$

This unit strength for a full-scale cube of the rock mass can then be adjusted for shape effect using the Obert-Duvall relation:

$$\sigma_p = \sigma_{S'}\left(0.78 + 0.22\frac{W}{H}\right) \quad (59.16)$$

Finally, the Hoek-Brown failure criterion can also provide an estimate of the strength for a full-scale cube of the rock mass. For most rock masses with good to reasonable quality,

$$\sigma_1' = \sigma_3' + \sigma_c\left(m_b\frac{\sigma_3'}{\sigma_c} + s\right)^a \quad (59.17)$$

where m_b, s and a are constants which depend on the rock mass quality, σ_c is the uniaxial compressive strength of the intact rock pieces (equivalent to σ_S), and σ_1' and σ_3' are the axial and confining principal stresses.

The constants m_b and s are estimated using a rock mass classification index called GSI, which is equivalent to Bieniawski's Rock Mass Rating (RMR) assuming a dry rock mass. See Hoek, Kaiser and Bawden (1995) for a complete discussion of the Hoek-Brown failure criterion for rock masses.

59.2.3 Barrier Pillar Design

The above pillar stress and pillar strength formulas apply mainly to pillars within a large array or so-called panel pillars. The barrier pillars surrounding this array of panel pillars also require sizing. Tributary area method can provide a conservative estimate of barrier pillar stress, if we assume that the panel pillars have all failed or else are all mined and therefore carry no overburden stress. Alternatively, numerical methods such as MULSIM/NL or LAMODEL can provide an estimate of barrier pillar load without making the conservative assumptions inherent to tributary area method.

The empirical pillar strength formulas shown earlier apply to pillars with a width-to-height ratio less than 5. For barrier pillars and other pillars in coal mines with a W/H ratio greater than 5, Salamon's "squat" pillar formula applies:

$$\sigma_p = \sigma_{S'}\left(\frac{5^b}{V_p{}^a}\right)\left(\frac{b}{e}\left(\left(\frac{W/H}{5}\right)^e - 1\right) + 1\right) \quad (59.18)$$

where e = 2.5, a = 0.0667 and b = 0.5933.

For hard rock and other noncoal mines, an equivalent squat pillar formula does not exist. It is necessary to extrapolate the Obert-Duvall relation to high W/H ratios or else use numerical methods and the Hoek-Brown failure criterion to estimate required barrier pillar size.

Koehler and Tadolini (1995) review no less than ten empirical and observational approaches to barrier pillar design in coal mines. Most methods calculate minimum barrier pillar width as a function of depth, and some include seam thickness. Coal strength is generally neglected. Equivalent empirical approaches to estimate barrier pillar size in noncoal mines do not appear to exist.

59.2.4 Summary of Traditional Strength-Based Pillar Design Methods

For room-and-pillar coal mining, the ARMPS method developed by Mark (1997a) applies. This method incorporates tributary area method and empirical strength formulas for sizing coal pillars during advance and retreat mining. The method also includes adjustments to the pillar stress for factors such as side loading from previously mined panels. The ARMPS method can also determine barrier pillar size. Again, an equivalent program does not appear to exist for noncoal room-and-pillar mining, but the ARMPS method would apply with suitable adjustments to the input parameters.

With the traditional strength-based pillar design methods, the user can determine panel pillar size and barrier pillar size, but these methods do not specify the panel dimension in any way. Operational considerations such as equipment and productivity set the panel width and usually set it as large as possible. Based on strength considerations alone, a narrow panel will require a narrow barrier pillar and a wide panel will require a wide barrier pillar. Rock mechanics factors do not enter the panel width determination with these methods. Maximum panel width may be determined by the size of air blast that an operation could withstand, but this is not a rock mechanics factor. Other rock mechanics considerations are needed to rationally determine maximum panel width along with panel pillar and barrier pillar sizes.

59.3 CASE HISTORIES OF PILLAR COLLAPSES

If the strength of a pillar in a room-and-pillar mine is exceeded, it will fail, and the load that it carried will transfer to neighboring pillars. The additional load on these pillars may lead to their failure and so forth. This mechanism of pillar failure, load transfer and more pillar failure can lead to the rapid collapse of very large mine areas. In mild cases, only a few tens of pillars might fail; however, in extreme cases, hundreds, even thousands of pillars can fail. This kind of failure has many names such as "progressive pillar failure," "massive pillar collapse," "domino-type failure," or "pillar run." Swanson and Boler (1995) coined the term "cascading pillar failure" or CPF to describe these rapid pillar collapses.

CPF can have catastrophic effects on a mine, and sometimes these effects pose a greater health and safety risk than the underlying ground control problem. Usually, the CPF induces a devastating air blast due to displacement of air from the collapse area. An air blast can totally disrupt the ventilation system at a mine by destroying ventilation stoppings, seals, and fan housings. Flying debris can seriously injure or kill mining personnel. The CPF might also fracture large volumes of rock in the pillars and immediate roof and floor, leading to the sudden release of large quantities of methane into the mine atmosphere. A methane explosion might result from the cascading pillar failure.

Figure 59.4 gives a simple illustration of cascading pillar failure. Figure 59.4A shows a series of 12 equal-sized pillars each subject to the same tributary area load. These pillars are assumed to be near their maximum load or strength. If two of the center pillars are weaker than average and fail, their load is transferred to the neighboring pillars causing their load to increase dramatically, as shown in Figure 59.4B. More pillars then fail as shown in Figure 59.4C, and even greater loads transfer to the surrounding

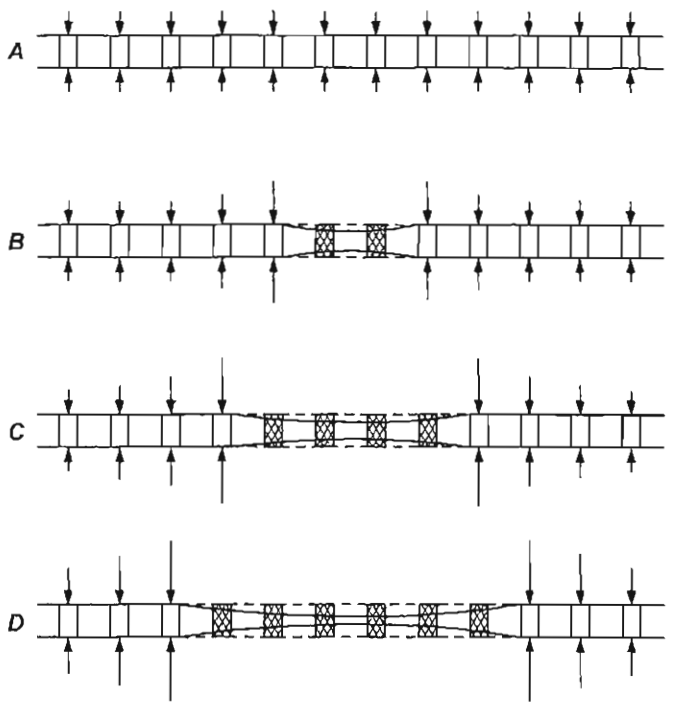

FIGURE 59.4 Simplified mechanics of cascading pillar failure or "CPF." Arrows indicate the relative magnitude of pillar load.

pillars as shown in Figure 59.4D. Thus, once the CPF has initiated, it becomes self-propagating. As shown in Figure 59.4, the loads on the intact pillars adjacent to the failure area increase as the extent of the failure increases, thereby driving the failure process even more. This process will continue until all pillars in the array have failed, or until a substantial barrier pillar or other solid abutment is reached.

The rapidity of these unstable pillar failures varies widely. At one end of the spectrum are slow "squeezes" that develop over days to weeks. Because of their slow progress, there is little immediate danger, and mining personnel and machinery have ample time to leave the vicinity safely. At the other end of the spectrum is cascading pillar failure, which can occur in a few seconds. With CPF, the failure occurs so rapidly that men and equipment do not have time to evacuate. Real danger of permanent entombment exists. Significant seismic energy is released as a result of the rapid failure and collapse. In addition, the rapid collapse is almost always associated with a potentially damaging air blast.

Many case histories exist of CPF in coal mines. The most infamous example is the Coalbrooke Colliery in South Africa where 437 miners perished when 2 square kilometers of the mine collapsed within a few minutes on January 21, 1960 (Bryan et al. 1966). Table 59.3 summarizes the mining dimensions of ten examples of rapid pillar collapse in coal mines. Most of these collapses occurred in the United States during the 1980s and 1990s except where noted. In all cases except Coalbrooke, these collapses happened suddenly or without any significant warning. All collapses resulted in substantial air blasts and severe damage to the ventilation system. Recent reports from India (Sheorey et al. 1995) and Australia (Galvin 1992) indicate that catastrophic pillar collapses and the associated air blasts have caused problems there as well.

Catastrophic pillar failures have also happened in many metal mines. Table 59.4 provides the mining dimensions of four room-and-pillar mines in the United States that most likely failed by the cascading pillar failure mechanism. The collapse areas can be huge. Fortunately, some of these failures gave advance warning. At the Bautsch mine, slabbing from pillars and roof falls began four weeks prior to the main collapse. At the copper mine considerable rock noise and smaller failures preceded the main collapse by five days. Visible signs of pillar deterioration and rock noise also preceded the failure at the lead mine. All of the collapses induced an air blast; however, due to the large room dimensions, damage to the ventilation systems was never severe. The only known damage occurred at the copper mine where several air doors were bent and a few stoppings were blown down.

The largest and most devastating examples of CPF occurred in nonmetal mines. Table 59.5 documents the mining dimensions of seven nonmetal mines that probably failed by the CPF mechanism. Substantial air blasts resulted from most of these collapses. The occurrence of warnings was divided. Rock noise and other failure warnings preceded the silica mine collapse by three weeks. Evidently, both trona mine collapses occurred without warning.

Mines experiencing a cascading pillar failure generally exhibit the following characteristics.

1. Extraction ratios are usually more than 60%. A high extraction ratio will put pillar stress close to peak strength and provide ample expansion room for the failed pillar material.
2. Width-to-height ratio of pillars is always less than 3 for coal mine failures, usually much less than 1 in the metal mine failures and less than about 2 for the nonmetal mine failures. A low W/H ratio ensures that the failed pillar material can easily expand into the surrounding openings and that the failed pillar will have little residual load bearing capacity.
3. The number of pillars across the panel width is always at least 5 and usually more than 10, which typically ensures that pillars have reached their full tributary area load. Minimum panel widths for CPF are at least 80 m.
4. Substantial barrier pillars with width-to-height ratios more than 10 are absent from the mine layout.
5. Depth covers the full range of mining conditions. Although CPF seems more prevalent in shallow mines less than 100 m deep, this may be due to the prevalence of shallow room-and-pillar coal mines.

59.4 MECHANICS OF CASCADING PILLAR FAILURE

In the simple explanation for CPF given earlier, rapid load transfer away from failing pillars is important in the failure mechanism. However, the underlying mechanics of CPF are more complex. The nature of the pillar failure process depends on the relative magnitude of certain mechanical properties of the rock mass and the pillar. Salamon's local mine stiffness stability criterion accounts for these properties and predicts whether the failure process will occur in a stable, nonviolent manner or in an unstable, violent manner. This section will explain this criterion and the mechanics of stable and unstable failure of rock, first in the laboratory, and then in a mine.

59.4.1 Stable and Unstable Failure of Rocks in the Laboratory

Prior to the 1960s, compression testing of rock specimens produced a load convergence curve similar to that shown in Figure 59.5A. Typical tests ended suddenly and violently upon arrival at or shortly after reaching the "ultimate load." Beyond some critical applied displacement (i.e., convergence), the specimen had no load-bearing capacity, usually because it had disintegrated completely. Early tests were done with so-called "soft" testing

TABLE 59.3 CPF examples in coal mines

Reference and year of collapse	Collapse area (m)	Depth (m)	% Extr.	Mining height (m)	Room width (m)	Pillar size (m)	W/H ratio	Panel width (m)	Airblast damage
Bryan et al. (1964) Coalbrooke 1960	2 km^2	140	56	4.3	6	12 × 12	2.8	210	437 miners killed
Ropchan (1991) Belina Mine 1991	300 × 450	170	56	5.8	6.1	12.2 × 12.2	2.1	170	Major, 1 injury
Chase et al. (1994) Case 1—1991	120 × 120	80	78	2.9	6.1	3 × 12.2	1.1	210	26 stoppings, 1 injury
Chase et al. (1994) Case 2—1990	90 × 120	75	78	3	6.1	3 × 12.2	1.0	150	40 stoppings
Chase et al. (1994) Case 3—1990	90 × 490	60	78	3	6.1	3 × 12.2	1.0	90–150	103 stoppings
Chase et al. (1994) Case 4—1992	120 × 150	70	64–75	3.3	6.1	6 × 6 9 × 9	1.8–2.7	180	37 stoppings
Mokgokong & Peng (1991) Emaswati Mine	60 × 140	60–140	75	3	6.1	12.2 × 12.2	2.0	80	Not known
Abel (1988) Roadside Mine 1983	200 × 400	210	84	2.1–2.4	6.1–12.2	3 × 24.4	1.3	430	Minor
Khair & Peng (1985)	120 × 120	90	75	2.1	6.1	6.1 × 6.1	2.8	120	Not known
Richmond (1998)	180 × 450	30–120	70	2.1	6.1	6.1 × 9.1	2.9	180	23 stoppings No injuries

TABLE 59.4 CPF examples in metal mines

Reference and year of collapse	Collapse area (m)	Depth (m)	% Extr.	Mining height (m)	Room width (m)	Pillar size (m)	W/H ratio	Panel width (m)	Airblast damage
Touseull & Rich (1980) Bautsch Mn. 1972	90 × 360	75	90	27	23	11 × 11	0.4	90	Minimal
Davidson (1987) Cu-Ag Mine 1987	90 × 120	300	60–65	20	14	9 × 90	0.5	150	Not known
Straskraba & Abel (1994) Copper Mine 1988	600 × 900	600	68	3.5–8.5	8.5	22 × 22 (A) 7 × 7 (R)	2.0–0.9	—	Minor
Dismuke et al. (1994) Lead Mine 1986	120 × 200	300	78	12	9.7	8.5 × 8.5	0.7	180	Minor

TABLE 59.5 CPF examples in non-metal mines

Reference and year of collapse	Collapse area (m)	Depth (m)	% Extr.	Mining height (m)	Room width (m)	Pillar size (m)	W/H ratio	Panel width (m)	Airblast damage
Swanson & Boler (1995) Trona Mine 1995	760 × 2,100	490	60–70	2.4–2.7	4.3	3.8 × 29	1.4	170	Major
Knoll (1990) Potash Mine 1989	6 km^2	700–900	45	6.1	10.7	30 × 30	5	—	Not known
Spruell (1992) Silica Mine 1992	75 × 90	18	56	12.2	6.1	9 to 15 ave. 12	1	—	Not known
Denk et al. (1994) Salt Mine 1993	200 × 200	330	92	3.7	16.5	5.5 × 5.5	1.5	200	None
No Reference Limestone Mine 1975	300 × 600	<60	>80	>6	15–30	5 to 15 irregular	—	300	Not known
No Reference Trona Mine 2000	760 × 340	490	70	2.4–2.7	4.3	3.8 × 29	1.4	170	Not known
No Reference Limestone Mine 2000	75 × 75	40–60	> 90	4–5	10	5 × 5	1	—	None

machines, and they produced only part of the load-convergence relationship for the specimen.

Modern compression testing with so-called "stiff" testing machines produces a complete load-convergence curve similar to the one shown in Figure 59.4.5B (Cook and Hojem 1966; Bieniawski 1967; Wawersik and Fairhurst 1970). A typical test does not end suddenly and violently at the ultimate load. The load on the rock first increases to ultimate and then decreases gradually. The rock specimen maintains its integrity and some load-bearing capacity even after the ultimate load is exceeded.

Jaeger and Cook (1979) discuss how confining pressure, temperature, loading rate, and other variables affect the shape of the stress-strain curve for a rock. For many practical mining engineering problems, the width-to-height ratio of a test specimen is of primary interest. Figure 59.6 from Das (1986) shows how the magnitude of peak strength, steepness of the post-failure portion

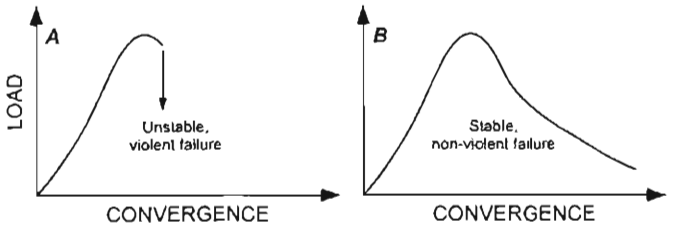

FIGURE 59.5 Typical load-convergence curves for rock from a "soft" testing machine (a) exhibiting unstable failure and from a "stiff" testing machine (b) exhibiting stable failure (Swanson and Boler 1995)

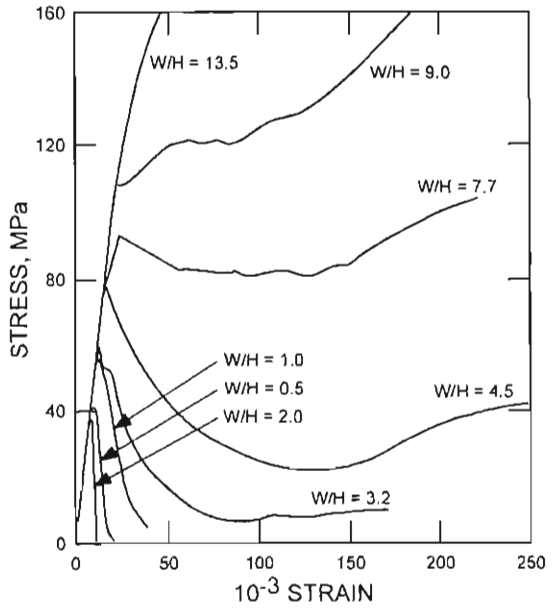

FIGURE 59.6 Complete stress-strain curves for Indian coal specimens showing increasing residual stength and post-failure modulus with increasing *W/H* ratio (Das 1986)

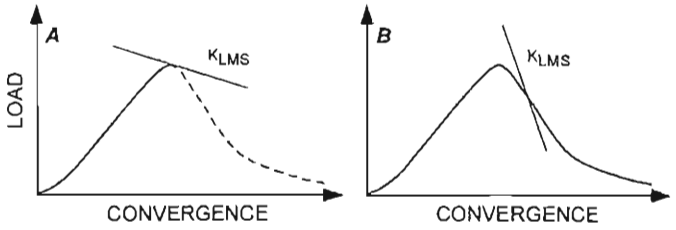

FIGURE 59.7 Unstable, violent failure versus stable, nonviolent failure. (A) loading machine stiffness is less than post-failure stiffnes sin a "soft" loading system. (B) loading machine stiffness is greater than post-failure stiffness in a "stiff" loading system (Swanson and Boler 1995).

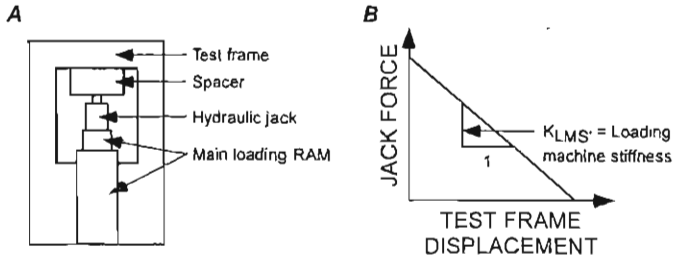

FIGURE 59.8 Illustration of scheme to measure loading machine stiffness. (A) pressurized jack replaces laboratory specimen in test frame; (B) loading machine stiffness is slope of jack force versus test frame displacement diagram.

of the stress-strain curve, and magnitude of the residual strength changes as the width-to-height ratio of a coal specimen increases. Specimen behavior is strain softening at first, then becomes elastic-plastic, and finally exhibits strain-hardening behavior as width-to-height ratio increases.

Salamon (1970) developed a criterion to determine whether the failure process observed in the laboratory occurs in a stable, nonviolent or in an unstable, violent manner. Figure 59.7 illustrates the criterion. Stable, nonviolent failure occurs when

$$|K_{lms}| > |K_p| \qquad \textbf{(59.19a)}$$

and unstable, violent failure occurs when

$$|K_{lms}| < |K_p| \qquad \textbf{(59.19b)}$$

where K_{lms} is the loading machine stiffness and K_p is the post-failure stiffness at any point along the load-convergence curve of the rock specimen. If the loading machine stiffness is less steep than the post-failure stiffness, as shown in Figure 59.7A, the failure is unstable and violent. However, if the loading machine stiffness is steeper than the post-failure stiffness, as shown in Figure 59.7B, the failure is stable and nonviolent. If the above failure criterion is violated, the specimen disintegrates at or just after reaching the ultimate load and only part of the load-convergence relation is observed. Satisfying the above stability criterion can result in measurement of complete load-convergence behavior of the specimen.

"Soft" and "stiff" testing machines differ in much more than just outward appearance. A stiff loading machine has a much larger steel reaction frame as well as a much larger hydraulic ram. However, the fundamental difference between "soft" and "stiff" testing machines that leads to stable or unstable specimen failure is in the way the loading machine itself reacts to induced load and stores energy during a compression test. Both the test specimen and the loading machine deform as the applied load increases. A "soft" testing machine will deform more than a "stiff" testing machine and thereby store more energy in the testing machine itself. Energy is stored in the test frame (the steel posts, the crosshead and any steel platens), the hydraulic ram and the hydraulic fluid. Therefore, if the load on a specimen is the same, a "soft" testing machine will store more energy (load times deformation) than a "stiff" testing machine. When the specimen reaches its maximum load-bearing capacity, the "soft" testing machine will relax and displace inward and thereby transfer all its stored strain energy to the specimen, which will lead to an unstable, violent failure. With a "stiff" testing machine operating in displacement control, the testing machine itself will not displace inward sufficiently to destroy the test specimen. Failure will occur in a stable, nonviolent manner, and it is possible to measure the complete load-convergence relation for the specimen.

Figure 59.8 shows a simple analogy to measure loading machine stiffness. In 59.8A, the rock specimen in the test frame is replaced with an equivalent, pressurized hydraulic jack. Relaxing

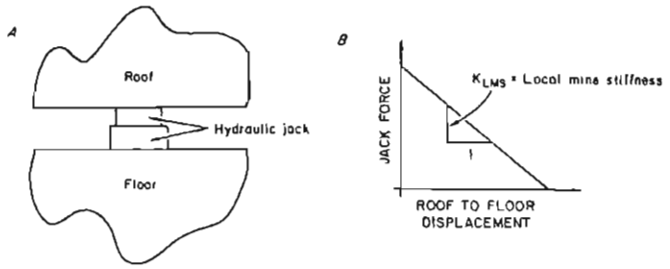

FIGURE 59.9 Illustration of scheme to measure K_{LMS}. (A) Jack replces mine pillar; (B) K_{LMS} is slope of jack force versus mine roof-to-floor displacement diagram.

the load on the jack causes the test frame to displace inward. The slope of the jack force versus test frame convergence relation, as shown in Figure 59.8B, is the loading machine stiffness.

59.4.2 Stable and Unstable Failure of Pillars in Mines

A rock specimen loaded in a laboratory test frame is analogous to a mine pillar loaded by the surrounding rock mass. Based on this analogy, Salamon's stability criterion (1970) also applies to mine pillars, and it will determine whether the failure process occurs in a stable, nonviolent or in an unstable, violent manner. Stable, nonviolent failure occurs when:

$$|K_{LMS}| > |K_P| \qquad \textbf{(59.20a)}$$

and unstable, violent failure occurs when

$$|K_{LMS}| < |K_P| \qquad \textbf{(59.20b)}$$

where K_{LMS} is the local mine stiffness and K_P is the postfailure stiffness at any point along the load-convergence curve of the pillar. The local mine stiffness, K_{LMS}, is an inverse load-convergence characteristic analogous to the loading machine stiffness, K_{lms}.

Similar to the means discussed earlier to measure loading machine stiffness, Figure 59.9 illustrates a means to measure K_{LMS} in a mine. The pillar is replaced by a large hydraulic jack (Figure 59.9A), which is then pressurized to simulate a loaded mine pillar. Relaxing the load on the jack causes the mine roof and floor to displace inward. The slope of this force-displacement relation, as shown in Figure 59.9B, is K_{LMS}.

The local mine stiffness depends on the modulus of the immediate roof, floor and pillar materials and the layout of pillars, mine openings and barrier pillars. Figure 59.10 shows how the local mine stiffness changes for different mine layouts, starting with a single pillar surrounded by wide openings, then an array of small pillars, and finally, a small pillar surrounded by barrier pillars. Consider the load-convergence response if a hydraulic jack replaces one small pillar and a unit load on the jack is released. For the case of a single pillar surrounded by wide openings, a unit-load decrease results in a large convergence increase. Therefore the local mine stiffness has a shallow slope as indicated by "B." In an array of small pillars, a unit-load decrease results in a smaller convergence increase, and the local mine stiffness has a steeper slope as shown by "C." Finally, if the small pillar is surrounded by large barrier pillars, a unit-load decrease results in a very small convergence increase, and the local mine stiffness is very steep as shown by "D." The worst case is that of "A" or dead weight loading, where the local mine stiffness is horizontal with zero slope. Such a local mine stiffness would always produce a violent failure if the pillars exhibit any strain softening behavior.

At this time, theory cannot predict the speed at which an unstable pillar failure will propagate. In other words, current rock mechanics theory does not predict whether an unstable failure will progress slowly, as a "squeeze," or rapidly as a CPF.

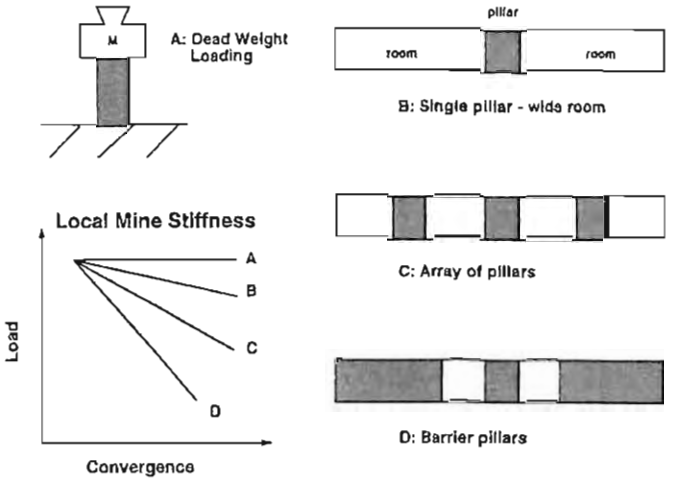

FIGURE 59.10 Relative local mine stiffness for various mine alyouts. Shaded pillar is analogous to hydraulic jack from Figure 59.9. Local mine stiffness magnitude as extraction increases (Swanson and Boler 1995).

The speed of failure might depend in part on the degree in which the local mine stiffness stability criterion is violated.

59.5 STABILITY-CRITERION-BASED PILLAR DESIGN METHODS

The traditional strength-based pillar design procedures discussed earlier consider only the peak strength of the pillar. If the applied stress on the pillar reaches this level, its safety factor against strength failure is 1. There is great economic incentive to design pillars with a low strength-safety factor because as the strength-safety factor decreases the extraction ratio increases along with resource recovery, mining revenues, and potential profits. The most economic pillar designs are necessarily very close to the peak strength, but still on the prefailure side of the complete load-convergence curve for the pillar. Because of the inherent variability in pillar strength, it is also important to consider what might happen to a particular room-and-pillar mine plan if some of the pillars exceed the peak strength and enter the postfailure portion of their complete load-convergence curve. Such considerations are necessary especially when the number of pillars in an array is large. In that case even if the average strength safety factor of the pillars is large, say 1.5, and their probability of failure is small, the probability of pillar failure somewhere in the array is likely to be large. Failure of just a few pillars in an array may be sufficient to initiate a CPF even if their average strength safety factor is large.

Engineers have known for some time about the strain-softening, postfailure behavior of rock and the implications of this behavior on mine safety. However, it is another matter to translate that knowledge into efficient, economic mine designs for extraction of bedded deposits using room-and-pillar and related mining techniques. The proposed methodology goes beyond using only traditional strength-based pillar design criterion and incorporates Salamon's local mine stiffness stability criterion for both sizing pillars and determining mine layout. On the basis of this stability criterion, three different approaches are proposed to control CPF—containment, prevention, and full extraction approach.

59.5.1 Containment Approach

In the containment approach, shown in Figure 59.11, an array of panel pillars, that violate the local mine stiffness stability criterion and can therefore fail in an unstable, violent manner if their

strength criterion is exceeded, are surrounded or "contained" by barrier pillars. The primary function of barrier pillars is to limit the potential failure to just one panel. Barrier pillars have a high *W/H* ratio, typically greater than about 10, and contain panel pillars with low *W/H* ratio, typically in the 0.5 to 2 range. It is a noncaving room-and-pillar method in that panel pillars are not meant to fail during retreat mining.

Two factors help decrease the risk of a instantaneous CPF. First, the barrier pillars tend to shield the panel pillars from full overburden stresses and thereby increase their strength safety factor and decrease their probability of failure. Second, if the panel pillars do fail, the failure will not propagate beyond the barrier pillars. A conservative approach is to size the barrier pillars on the assumption that all the panel pillars within have failed. Most important though, barrier pillars must have a sufficiently large *W/H* ratio to eliminate any strain-softening behavior.

If an engineer chooses to use panel pillars with a low *W/H* ratio that exhibit strain-softening behavior and can violate the local mine stiffness stability criterion, then it is imperative to limit panel sizes and surround all panels with adequate barrier pillars. The load transfer method presented by Abel (1988) provides an approach for estimating maximum panel width. Use of this method will help insure that panel pillars never experience full tributary area stress. Even though barrier pillars shield panel pillars from full tributary area stress, the small pillars should have the ability to withstand this maximum stress.

To summarize, the main design characteristics of the containment approach are:

1. Panel pillars have a low strength safety factor (usually between 1.1 to 1.5) and low *W/H* ratios (usually less than 3 or 4). The panel pillars violate the local mine stiffness stability criterion and can therefore fail violently.
2. Barrier pillars have high *W/H* ratios (usually greater than 10) and do not exhibit any strain softening behavior. Therefore, they cannot fail violently. Barrier pillars also have sufficient strength to remain intact even if all pillars within a panel should fail.
3. The minimum load transfer distance limits panel width to insure that panel pillar stresses are less than full tributary area stresses.
4. Panel sizes are also limited by the maximum air blast size that the mine layout can withstand should CPF occur within a panel.

59.5.2 Prevention Approach

In contrast to the containment approach, the prevention approach "prevents" CPF from ever occurring by using panel pillars that satisfy both the local mine stiffness stability criterion and a strength criterion. Therefore, the panel pillars cannot fail violently, and CPF is a physical impossibility. Strictly speaking, this approach may not need barrier pillars to insure overall stability against CPF; however, their use is still advisable. To satisfy the local mine stiffness stability criterion, the panel pillars will usually have high *W/H* ratios (greater than about 3 or 4) and high strength safety factors as well (greater than 2). Another approach to increase the local mine stiffness and satisfy the stability criterion is to limit the panel width with properly spaced and sized barrier pillars.

Figure 59.12 illustrates the prevention approach for another typical advance and retreat mining sequence. In this example, a modification to the retreat mining system leaves remnant pillars with higher *W/H* ratio and more desirable postfailure characteristics that satisfy the local mine stiffness stability criterion. As with the containment approach, it is a noncaving room-and-pillar system.

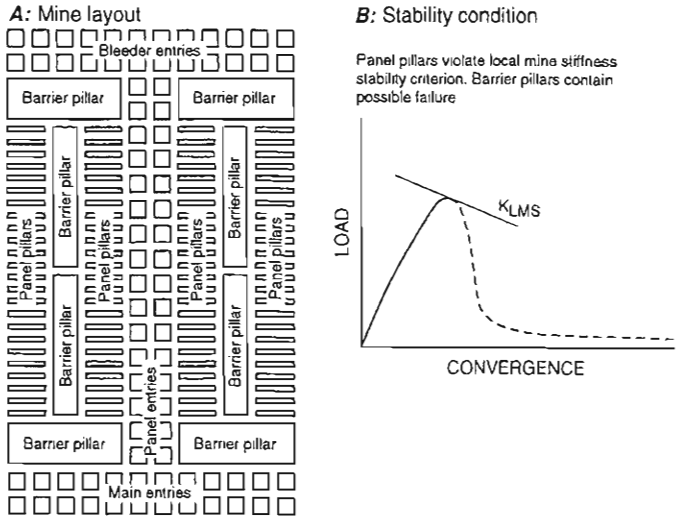

FIGURE 59.11 Containment approach to room-and-pillar mine layout: (A) pillar failure is 'compartmentalized'; (B) stability condition is such that pillar with low *W/H* ratio violate local mine stiffness stability criterion; panel pillars can, therefore, fail violently, but adequate barrier pillars that restrict spread of unstable failure surround them. Extraction for layout shown in 59%.

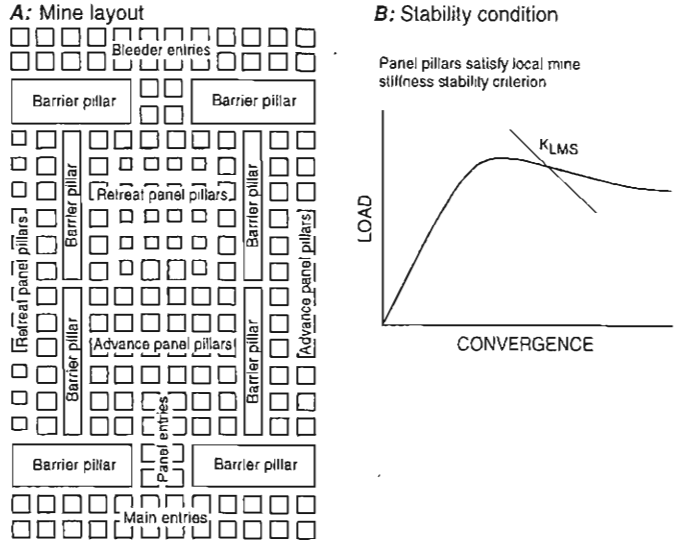

FIGURE 59.12 Full extraction approach: (A) failure of pillar remnants along with overburen occurs immediately after pillar extraction: (B) retreat mining must ensure development of sufficiently weak remnant pillars. Extraction for layout shown in 67%.

59.5.3 Full Extraction Approach

The full extraction approach shown in Figure 59.13 avoids the possibility of CPF altogether by ensuring total closure of the opening and full surface subsidence on completion of retreat mining. This approach does not require barrier pillars for overall panel stability; however, they are needed to isolate extraction areas and protect mains and bleeders. The main design characteristics of a full extraction approach are:

1. Panel pillars on advance must have adequate strength safety factors (greater than about 2).

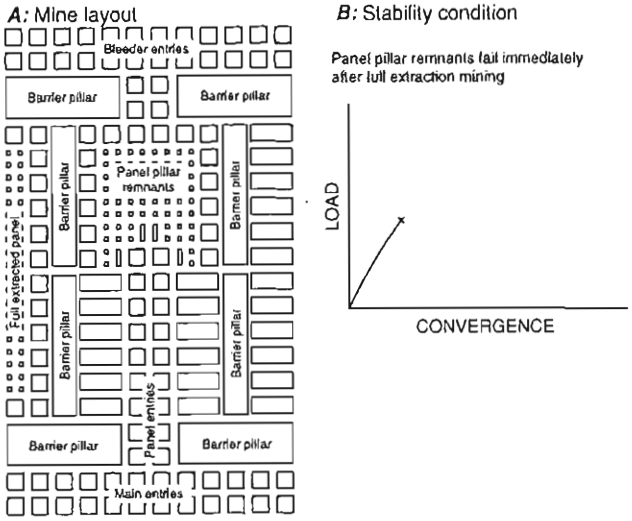

FIGURE 59.13 Full extraction approach: (A) failure of pillar remnants along with overburden occurs immediately after pillar extraction: (B) retreat mining must ensure development of sufficiently weak remnant pillars. Extraction for layout shown is 67%.

2. In addition, panel pillars should satisfy the local mine stiffness stability criterion during advance mining by having high W/H ratios (greater than about 4).
3. Panel pillars on retreat must have strength safety factors much less than 1 to ensure their complete collapse soon after retreat mining.

59.6 NUMERICAL SIMULATION OF CASCADING PILLAR FAILURE

59.6.1 Boundary-Element-Method Implementation

The NIOSH (former USBM) boundary element program called MULSIM/NL was modified to evaluate the local mine stiffness stability criterion and simulate the mechanics of CPF. MULSIM/NL calculates stresses and displacements using a displacement-discontinuity approach, which applies especially well to thin, bedded-type deposits such as coal and certain metals. The in-seam materials can follow a strain-softening constitutive model. This strain-softening model enables the simulation of CPF.

MULSIM/NL calculates the local mine stiffness (K_{LMS}) around a pillar as

$$K_{LMS} = \frac{(S_u - S_p)A}{(D_u - D_p)} \tag{59.21}$$

where

S_u = unperturbed stress at an element,
S_p = perturbed stress at an element,
D_u = unperturbed displacement at an element,
D_p = perturbed displacement at an element, and
A = element area.

The local mine stiffness for the pillar is the summation of all the stiffnesses composing the pillar. The unperturbed stresses and displacements are calculated in the usual way with MULSIM/NL. The perturbed stresses and displacements are then calculated by first removing the pillar where K_{LMS} is desired and then resolving for stresses and displacements. In this approach, S_p is identically 0.

TABLE 59.6 Unstable and stable model characteristics

	Unstable model	Stable model
Grid size	90 × 90	90 × 90
Element width (m)	3	3
Pillar height (m)	3	3
Depth (m)	80	160
Applied stress (MPa)	2	4
Rock mass modulus (MPa)	3,500	7,000
Coal modulus (MPa)	3,500	3,500
Pillar W/H ratio	1	3
Extraction on advance	59.1%	49.0%
Extraction on retreat	79.6%	81.6%

The minimum postfailure stiffness (K_P) for the pillar is calculated as

$$K_P = \frac{E_P A}{t} \tag{59.22}$$

where

E_P = postfailure modulus for material model,
A = element area, and
t = element thickness.

The postfailure stiffness for the pillar is then the sum of all element stiffnesses making up the pillar.

Based on these calculations of local mine stiffness and postfailure stiffness, the modified MULSIM/NL program applies the local mine stiffness stability criterion and ascertains the nature of the likely failure process, either stable or unstable. Depending on whether the criterion is satisfied or violated, the stress and displacement calculations with MULSIM/NL behave in vastly different manners.

59.6.2 Example Unstable and Stable Numerical Simulations

Two simple models of coal mines, one stable and the other unstable, demonstrate the local mine stiffness criterion and its influence on numerical model behavior. These calculations demonstrate the feasibility of calculating pillar stresses for traditional strength-based pillar design and evaluating the local mine stiffness for stability-criterion-based pillar design. Table 59.6 gives the basic model characteristics.

Figure 59.14 shows complete strain-softening, stress-strain curves for coal pillars with different W/H ratios as used in these simulations (Zipf 1999). The peak strengths in these curves are consistent with the coal pillar strength formulas summarized by Mark and Iannacchione (1992). The postfailure moduli approximate field data presented by Bieniawski (1968b), Van Heerden (1975) and Wagner (1974). Finally, the residual strength values for these full-scale pillar stress-strain curves are an estimate based on limited field data and observed laboratory-scale data.

The mine geometry for the stable and unstable models is visible in the resulting stress and displacement analyses. In the unstable model (Figure 59.15), advance mining develops 6 m by 27 m pillars and 6-m-wide rooms. On retreat, 3 m by 27 m pillars are left for an overall extraction of almost 80%. These pillars have a W/H ratio of 1 and follow the corresponding stress-strain curve shown in Figure 59.14. In the stable model (Figure 59.16), advance mining creates 15-m-square pillars with 6-m-wide rooms. On retreat, 9-m-square pillars are left to achieve an overall extraction of about 82%. However, these pillars have a W/H ratio of 3, and as shown in Figure 59.14, have a higher strength and different postfailure characteristics.

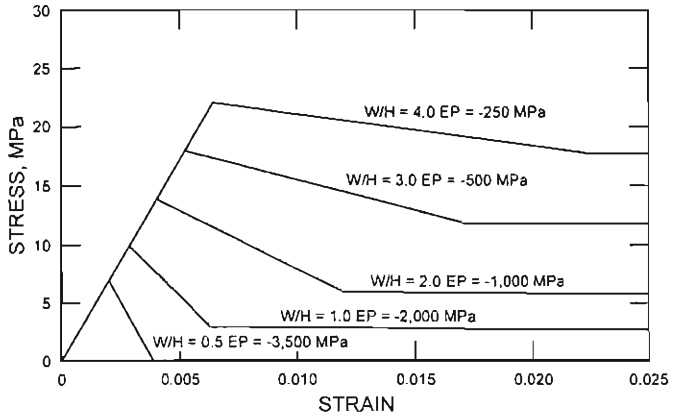

FIGURE 59.14 Strain-softening, stress-strain curves for coal pillars with increasing *W/H* ratio. E_P is minimum postfailure modulus.

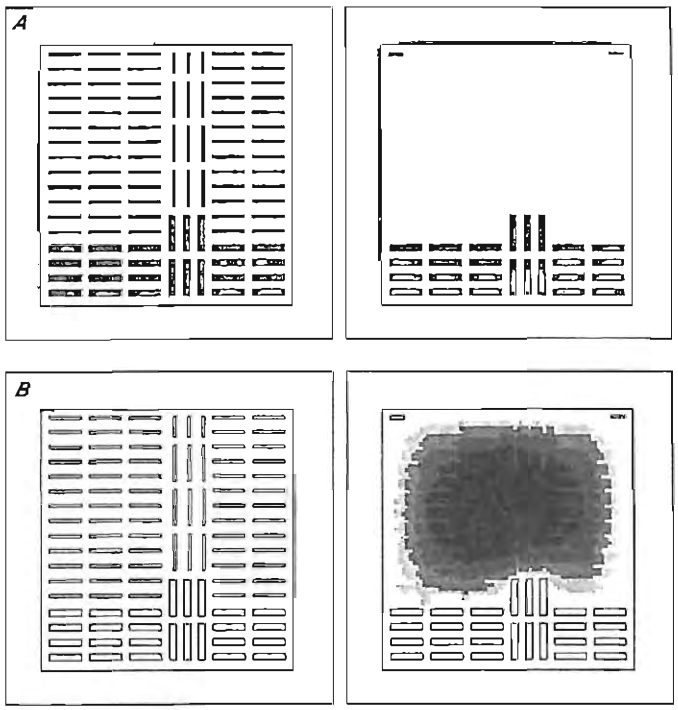

FIGURE 59.15 Unstable case, (A) stress and (B) convergence before and after pillar weakening. Light to dark gray indicates increasing magnitude of calculated vertical stress and convergence.

Each model has two mining steps. In the first step, the applied vertical stress brings the pillars close to failure. For the unstable case, a vertical stress of 2 MPa results in an average pillar stress of about 8.7 MPa, which implies a strength safety factor of about 1.15 for these pillars with a *W/H* ratio of 1. In the stable case, applying a vertical stress of 4 MPa results in an average pillar stress of 17.2 MPa and a strength safety factor of 1.05 for these pillars with a *W/H* ratio of 3.

In the second mining step, each model is perturbed artificially. For the unstable case, 3 pillars in the middle of the array of 77 pillars are weakened by decreasing their peak strength by 10% from 10 down to 9 MPa. In reality, this strength decrease could stem from creep or an undersized pillar. This small disturbance though is enough to trigger a CPF. Figure 59.15 shows the

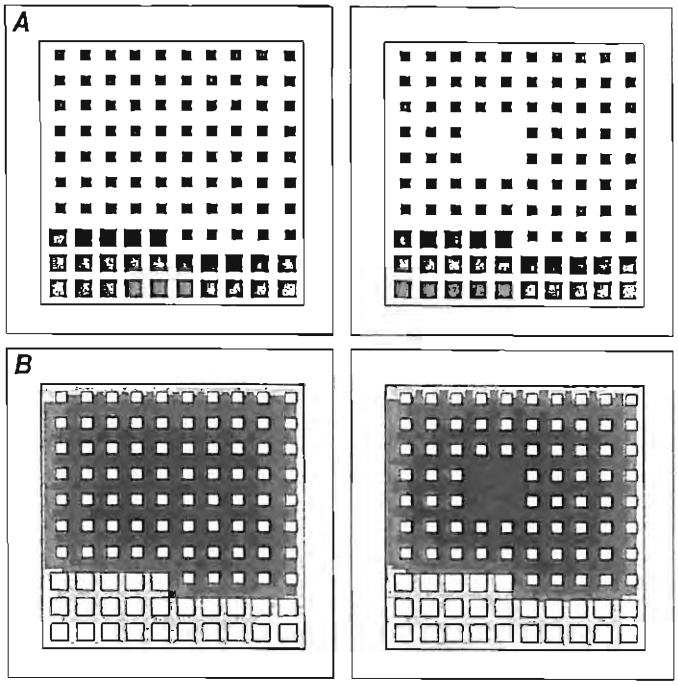

FIGURE 59.16 Stable case, (A) stress and (B) convergence before and after pillar removal. Light to dark gray indicates increasing magnitude of calculated vertical stress and convergence.

computational results. The stresses in the small pillars shown in Figure 59.15A are near their peak stresses of 10 MPa prior to the CPF, and they decrease to their residual level of 3 MPa after the failure. Convergence shown in Figure 59.15B is small before pillar weakening and increases dramatically after the CPF. In an unstable-type failure, Figure 59.15 shows that a small disturbance or a small increment of mining can result in a much, much larger increment of failure.

The unstable case violates the local mine stiffness stability criterion given by Equation 19. In mining step 1 where all the small pillars are near failure, K_{LMS} calculated by removing one pillar is −7,700 MN/m while the post-failure stiffness for that pillar is −54,000 MN/m. Therefore, unstable failure is possible by the stability criterion. In mining step 2, failure is already complete. K_{LMS} for this pillar is computed as −21,500 MN/m. Again, the stability criterion is violated and unstable failure is possible; however, it has already occurred.

For the stable case, a more radical disturbance is perpetrated by removing 4 pillars from the array of 75 pillars. Even though this disturbance is far greater than the pillar weakening done in the unstable case, a CPF does not result. Rather, stable progressive failure of the surrounding pillars takes place. Figure 59.16 shows the numerical model calculations. Some of the stresses shown in Figure 59.16A are already post-peak before pillar removal. After pillar removal, the size of the area and the number of pillars in the postfailure regime increase; however, the increase is not radical. The convergence shown in Figure 59.16B increases after pillar removal; however, that increase is not catastrophic as in the unstable case shown in Figure 59.15B. In contrast to the previous case of unstable failure, Figures 59.16A and 59.16B show that in stable failure, a disturbance or some increment of additional mining results in a more or less equal increment of additional failure in the model.

The stable case satisfies the local mine stiffness stability criterion given by equation 19. In mining step 1, K_{LMS} calculated by removing one pillar is −34,400 MN/m, and the postfailure

stiffness for that pillar is −13,500 MN/m, which implies stable failure. In mining step 2, K_{LMS} decreases in magnitude to −32,100 MN/m; however, stable failure still prevails.

59.6.3 Behavior of Local Mine Stiffness Calculations

Initial research with practical K_{LMS} calculations indicates that K_{LMS} tends to decrease in magnitude significantly as the peak strength of an array of pillars is approached, and then increase after failure is complete. The differences in K_{LMS} stem from whether the perturbation used for the K_{LMS} calculation is sufficient to initiate the CPF itself. At lower vertical stress and higher strength safety factor for an array of pillars, removal of one pillar is not sufficient to precipitate CPF, and K_{LMS} has a relatively high magnitude. When the pillar array is near failure and strength safety factor is near 1, removal of one pillar to calculate K_{LMS} initiates CPF in the model. Perturbed displacements calculated by the model increase dramatically; and therefore, K_{LMS} decreases in magnitude significantly. K_{LMS} calculations at a pillar within a failed array then seem to increase in magnitude back to the low stress, prefailure values. The magnitude of the decrease appears to be on the order of 3.

This decrease in K_{LMS} magnitude near and during failure has important implications in the mechanics of CPF and in design practices to eliminate it. As Swanson and Boler (1995) point out, once a CPF is initiated and K_{LMS} decreases in magnitude, violation of the local mine stiffness stability criterion becomes even more acute. Thus, once the CPF gets going, it becomes more self-propagating and more difficult to arrest the more it grows. It is possible that mine layouts that apparently satisfy the stability criterion, such as the stable case in the example above, could become unstable and CPF could result if the mine layout is disturbed by a sufficiently large "kick." In the unstable case, initial research shows that K_{LMS} could decrease in magnitude by a factor of 3 during the failure process. Accordingly, this decrease suggests that using a "safety factor" of at least 3 is necessary when applying the local mine stiffness stability criterion. Further research on K_{LMS} calculations is suggested in this area.

59.7 ANALYSES OF CASCADING PILLAR FAILURE CASE HISTORIES

Three recent case histories of CPF in mines are analyzed with numerical models, which calculate stress and convergence before and after catastrophic failure. In each model, best estimates and/or assumptions are made for the strain-softening properties of the pillars. Local mine stiffness is calculated, and the stability criterion is evaluated to show how each case most likely violated this criterion, and a CPF resulted.

59.7.1 Case History 1—Coal Mine Collapse

Chase et al. (1994) document this case history of massive pillar collapse or CPF in a coal mine. Table 59.7 summarizes the important characteristics of the boundary-element-method model of this mine. The stress-strain curves for coal shown in Figure 59.14 are applied in this model. Figure 59.17 shows the layout for the coal mine model. Using 6-m-wide rooms, a system of 12-m-square pillars with a W/H ratio of 4 were developed on advance. On retreat, these pillars were split down the middle with a 6-m-wide room to leave two 3-m-wide fenders with a W/H ratio of 1. The mine had split about nine rows of pillars with this method when CPF occurred causing seven rows of fenders to fail. The idealized numerical model contains just seven rows of fenders.

In the two-step model, the applied vertical stress of 2.3 MPa loads the fenders close to their peak strength of 10 MPa. Average pillar stress is about 9.3 MPa, which implies a safety strength factor of 1.08. In the second mining step, peak strength is decreased from 10 down to 9 MPa to weaken 8 fenders in the array of 138. This artificial weakening simulates time-dependent strength loss. This disturbance is sufficient to initiate the CPF.

TABLE 59.7 Case history 1—Coal mine collapse model characteristics

Grid size	90 × 100
Element width (m)	3
Pillar height (m)	3
Depth (m)	90
Applied stress (MPa)	2.3
Rock mass modulus (MPa)	6,000
Coal modulus (MPa)	3,500
Pillar W/H ratio—advance	4
Pillar W/H ratio—retreat	1
Extraction on advance	55.6%
Extraction on retreat	77.8%

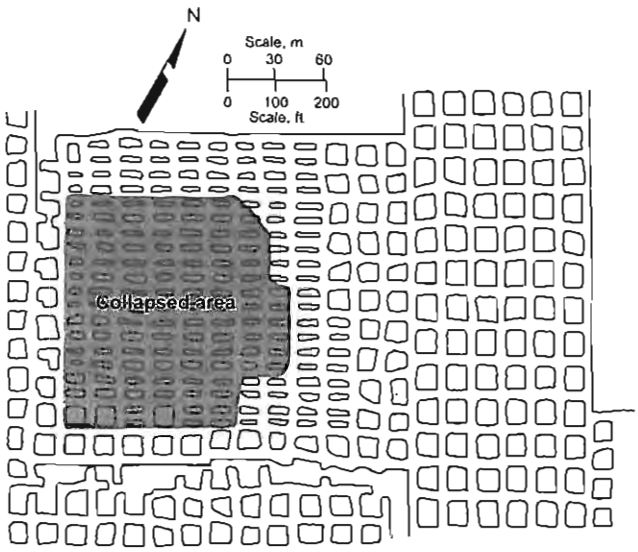

FIGURE 59.17 Mine layout for case history 1—coal mine collapse

Figures 59.18 and 59.19 show the stress and convergence before and after the failure. Stresses decrease from values near the peak stress to residual values while convergence increases dramatically. As in the previous unstable simulation, a small disturbance or increment of mining triggers a very large increment of failure in the model.

This case history apparently violates the local mine stiffness stability criterion. K_{LMS} is calculated as −6,600 MN/m during the first step and −19,700 MN/m during the second. Post-failure stiffness is −24,000 MN/m; therefore, unstable failure is possible by the criterion. Because the model is near failure under the 2.3 MPa vertical stress, computing K_{LMS} by removing a pillar precipitates the CPF. Again, the K_{LMS} value calculated during the failure process is about 1/3 less in magnitude than values calculated well before or well after failure.

59.7.2 Case History 2—Evaporite Mine Collapse

Swanson and Boler (1995) and Zipf and Swanson (1999) describe the mine geometry and aftermath of the collapse analyzed. Figure 59.20 shows the layout for this evaporite mine. During advance mining, a system of chain pillars is developed off a set of mains. At the same time, rooms are mined down the one side leaving long narrow panel pillars with a W/H ratio of 1.33 and a small interpanel pillar with a W/H ratio of about 2.66. On retreat, additional rooms are mined on the other side of the chain

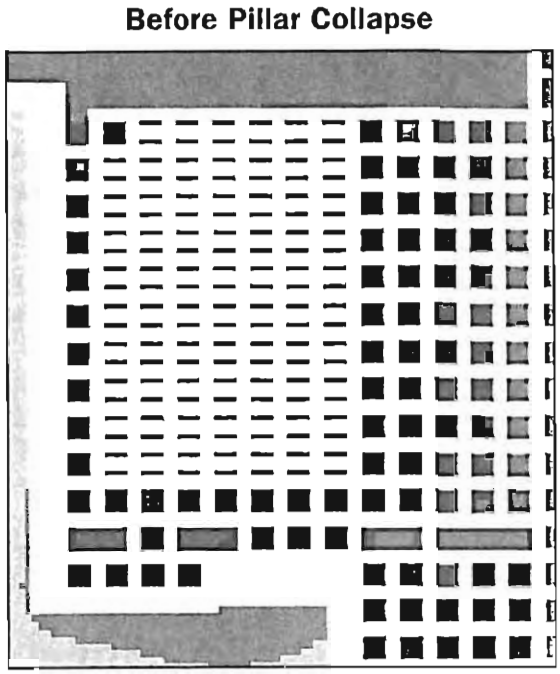

FIGURE 59.18 Coal mine stress before and after CPF. Light to dark gray indicates increasing magnitude of vertical stress.

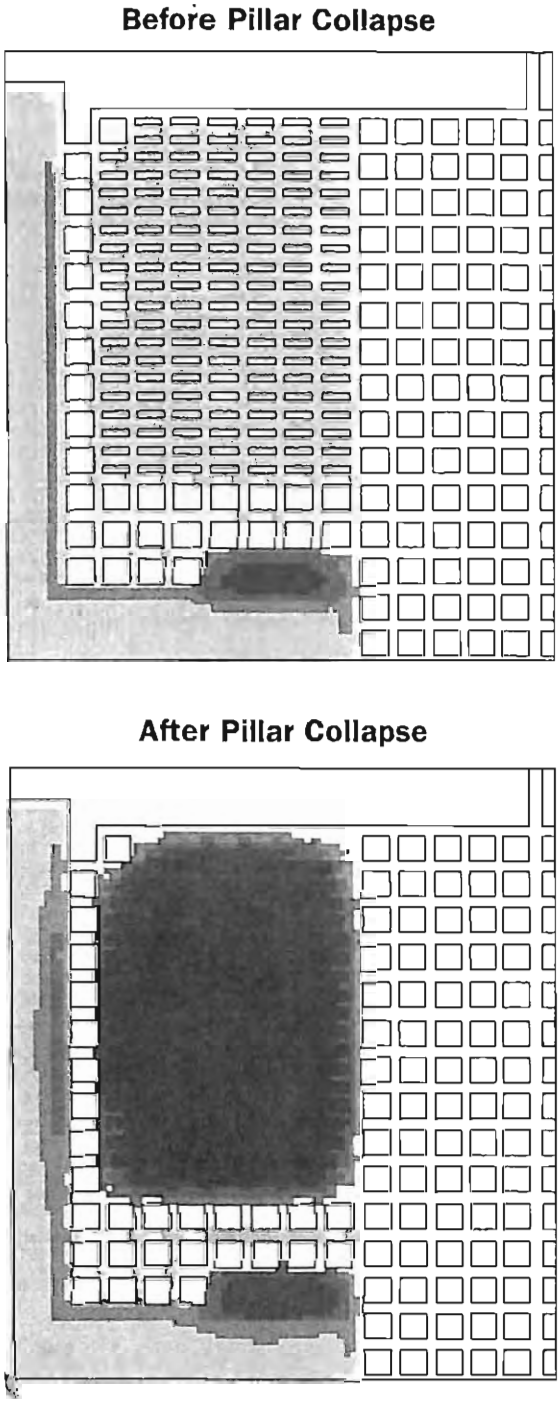

FIGURE 59.19 Coal mine convergence before and after CPF. Light to dark gray indicates increasing mgnitude of convergence.

pillars. In the actual mine layout, room width is 4.3 m, and the panel pillars are 3.8 m wide. The mine achieves an overall extraction of about 60% and extraction within a panel can be a little more than 70%.

Table 59.8 summarizes key input parameters for simple boundary-element-method models of this collapse. Due to the constant element size restriction, both room and panel pillar width are 4 m in the model. This approximation results in an extraction of 50% in the model.

In comparison to the available data for coal pillars, very little data exists for the complete stress-strain behavior of pillars in various metal and nonmetal mines. Direct measurements of the complete stress-strain behavior of pillars are difficult, very expensive, and often simply not practical. Laboratory tests on specimens with various *W/H* ratios can provide useful insights similar to the coal data shown earlier in Figure 59.6. MSHA (1996) used FLAC (Itasca 1995) to calculate the complete load-deformation behavior of the pillar-floor system in this evaporite mine. The objective of this modeling effort was to estimate post-failure stiffness of the pillar-floor system for a variety of pillar *W/H* ratios. Figure 59.21 shows the basic model geometry for these FLAC models. Each contained the same sequence of strong shale in the roof, strong

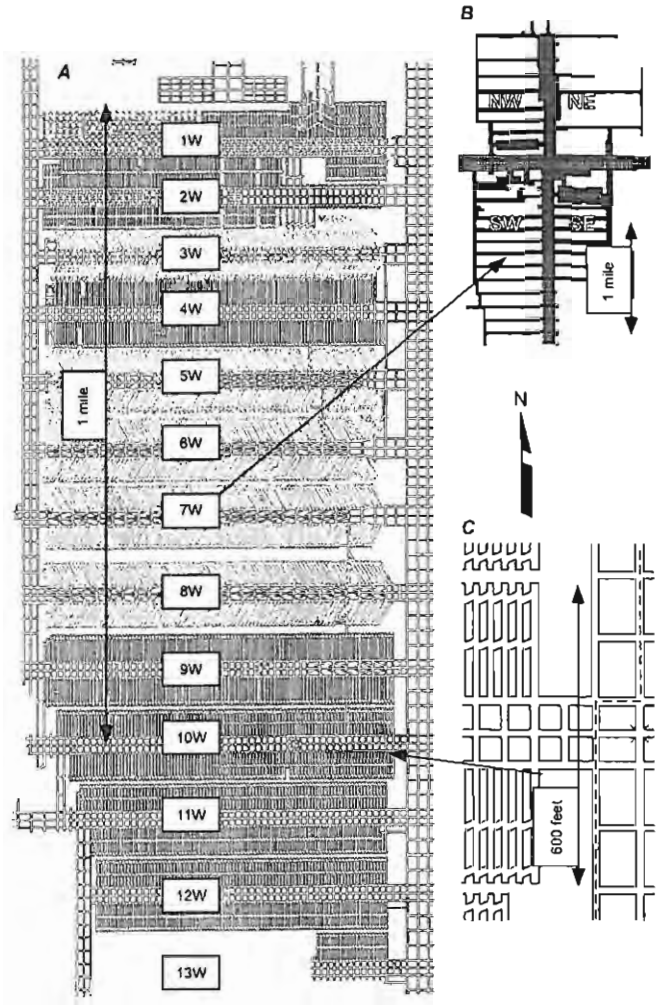

FIGURE 59.20 Mine layout for case history 2—evaporite mine collapse. (A) overall layout for part of the mine, (B) layout of southwest panels that collapsed and (C) details of a typical panel (MSHA, 1996).

TABLE 59.8 Case history 2—Evaporite mine collapse model characteristics

Grid size	120 × 120
Element width (m)	4
Pillar height (m)	3
Depth (m)	520
Applied stress (MPa)	13
Rock mass modulus (MPa)	3,500
Pillar modulus (MPa)	10,000
Pillar *W/H* ratio	1.33
Extraction (of model)	50%

and weak layers of the evaporite, a thin, strong oil shale layer in the immediate floor and a very weak mudstone deeper into the floor. Strain-softening material models were employed for each layer.

Figure 59.22 shows the computed rock movement after considerable deformation has occurred. The failure mechanism involves pillar punching through the thin, strong oil shale layer into the weak subfloor where a classic circular-arc-type failure

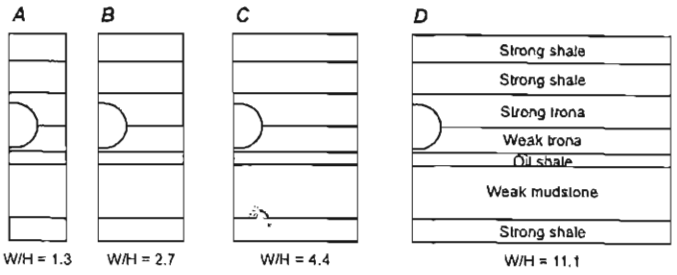

FIGURE 59.21 FLAC models of pillar-floor system for increasing pillar width and *W/H* ratio

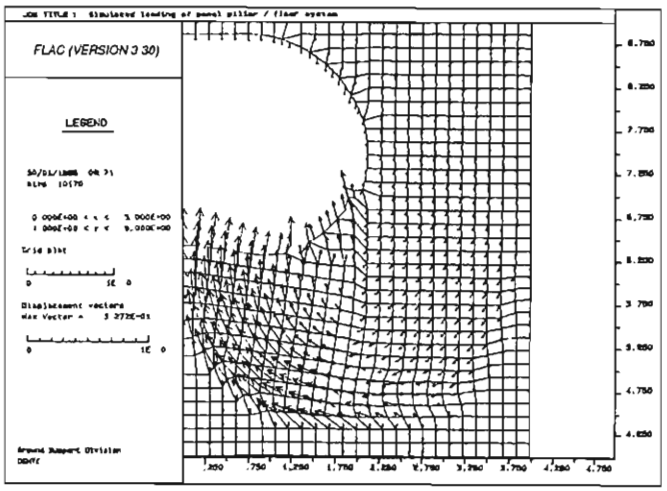

FIGURE 59.22 Computed rock movement after considerable deformation has occurred

develops. The computed failure mechanism matches field observations qualitatively; however, the computed deformations are much smaller than those observed in the field. This difference may arise because FLAC uses a continuum formulation to model a process that gradually becomes more and more discontinuous.

These computations provide an estimate of the complete stress-strain behavior of the overall pillar-floor system. Using the "history" function within FLAC, the model recorded average stress across the middle layer of the pillar and the relative displacement between the top and bottom of the pillar from which strain was computed. Figure 59.23 shows the effective stress-strain curves determined for the pillar-floor system from these four models. The initial post-failure portion of these curves provides an estimate of K_P for use in the local mine stiffness stability criterion. As stated earlier, computed displacements are smaller than observed, so the effective modulus and stiffness is also lower than indicated by these continuum-based computations. Figure 59.24 shows the strain softening, stress-strain relations as used in the boundary element models of the pillar collapse. These curves merely represent a best estimate of actual pillar-floor system behavior.

The BEM model in this analysis has two mining steps. The applied vertical stress of 13 MPa in the first mining step brings the long panel pillars close to failure. Average stress in these pillars is calculated as about 30 MPa. Since the peak strength of these pillars as shown in Figure 59.24 is 37 MPa, the safety factor of these pillars is about 1.2. In many circumstances, this safety factor may seem reasonable for many room-and-pillar mining applications. In the second mining step, 8 panel pillars in the array of 184 pillars are weakened by 15%. The artificial

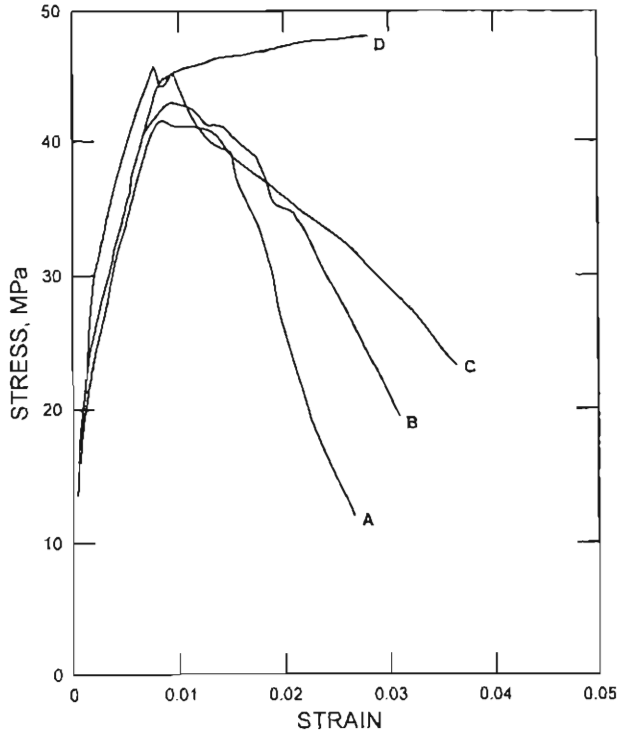

FIGURE 59.23 Stress-strain behavior of pillar-floor for increasing pillar width and *W/H* ratio

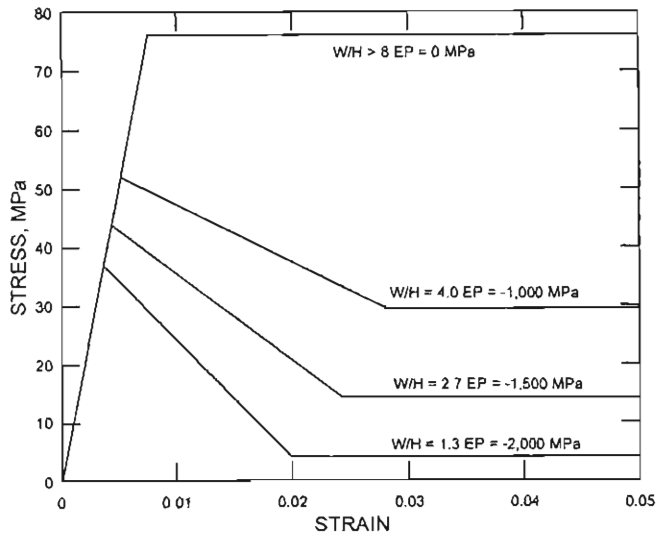

FIGURE 59.24 Strain-softening stress-strain curves for pillar/floor system with increasing pillar W/H ratio used in boundary-element-method analysis

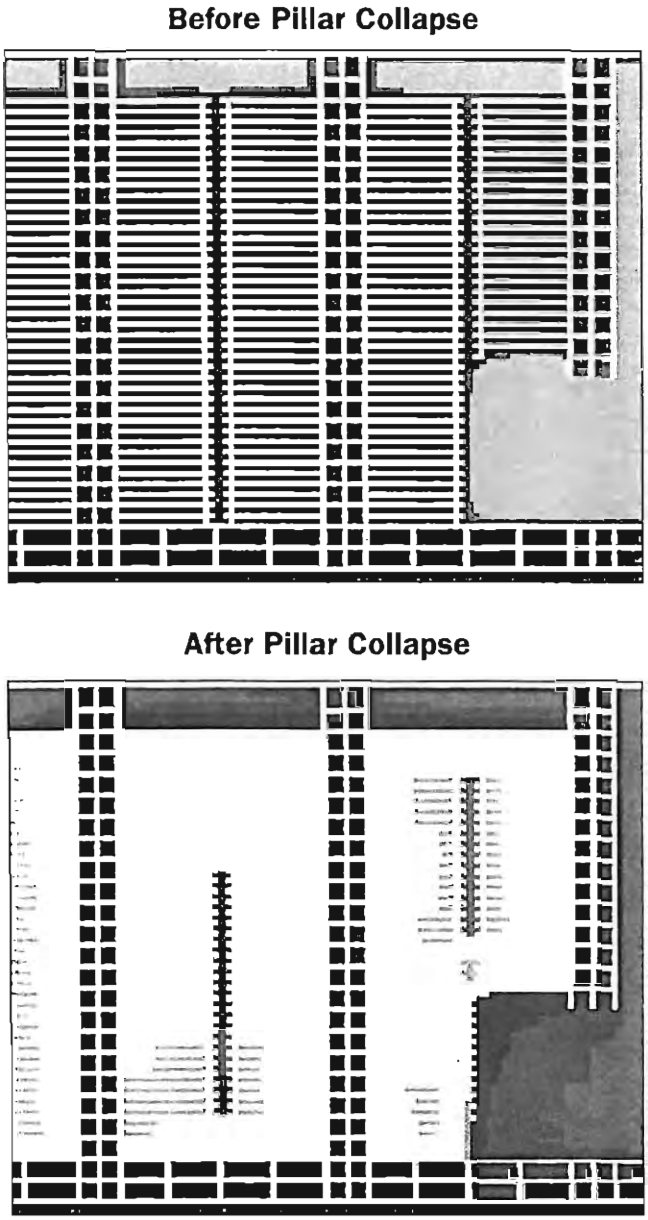

FIGURE 59.25 Evaporite mine stress before and after CPF. Light to dark gray indicates increasing magnitude of stress.

weakening approximates time-dependent strength loss. This small disturbance on about 4% of the panel pillars triggers the CPF.

Figures 59.25 and 59.26 present calculated stress and convergence before and after the CPF. The model shows that stresses shift to the perimeter of the collapse area while convergence increases dramatically in the middle. Once again, disturbance of a small area in the model leads to widespread failure.

K_{LMS} calculations suggest that this layout violates the local mine stiffness stability criterion. At one particular panel pillar, K_{LMS} is estimated as −60,420 MN/m during the first step before pillar weakening. After CPF is complete, K_{LMS} is −42,520 MN/m. Postfailure stiffness for the panel pillars is calculated as −170,700 MN/m. Therefore, unstable failure is a possibility by the local mine stiffness stability criterion. Again, good data on the postfailure behavior of the long panel pillars and the pillar-floor composite is limited. However, the simple assumptions and numerical analysis presented here support the hypothesis that CPF resulted because the local mine stiffness stability criterion was violated.

59.7.3 Case History 3—Metal Mine Collapse

Dismuke et al. (1994) describe this large pillar collapse in a major section of a room-and-pillar base metal mine. Figure 59.27 shows the collapse area. The failure began in four centrally located pillars and spread rapidly to include almost 100 pillars. Table 59.9

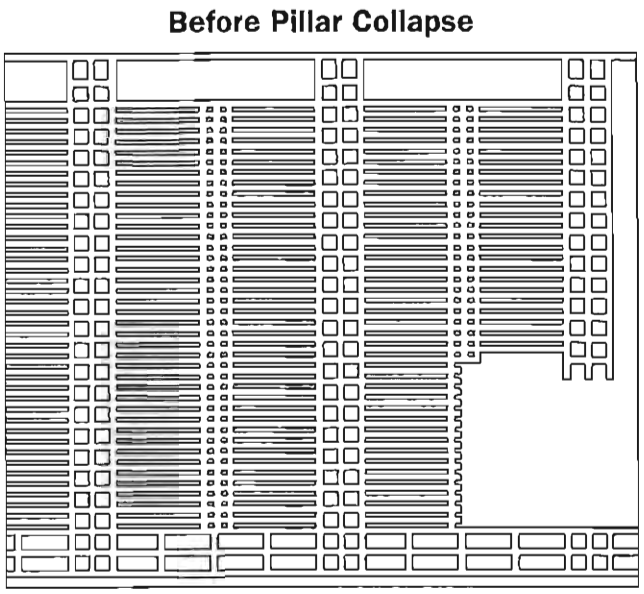

FIGURE 59.26 Evaporite mine convergence before and after CPF. Light to dark gray indicates increasing magnitude of convergence.

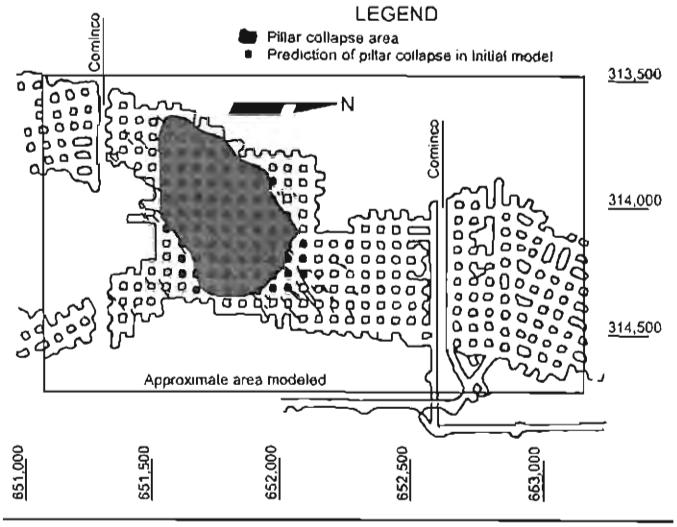

FIGURE 59.27 Mine layout for case history 3—metal mine collapse (Dismuke et al. 1994)

TABLE 59.9 Case history 3—Metal mine collapse model characteristics

Grid size	270 × 360
Element width (m)	1.21
Pillar height (m)	12.12
Depth (m)	300
Applied stress (MPa)	7.5
Rock mass modulus (MPa)	40,000
Pillar modulus (MPa)	40,000
Pillar *W/H* ratio	0.7
Extraction	80%

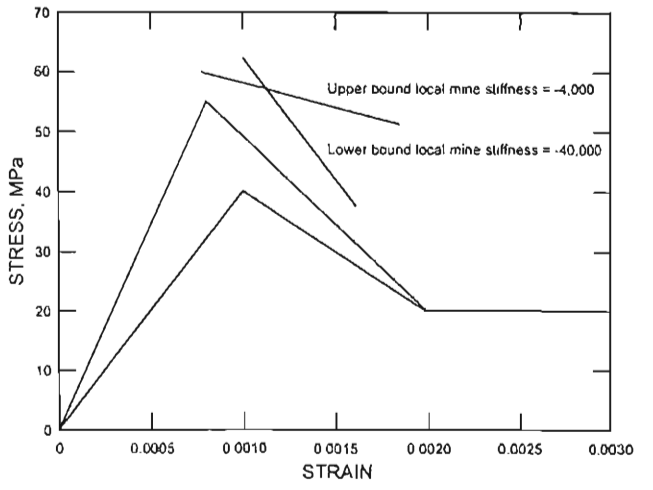

FIGURE 59.28 Stress-strain curves for 12.1- and 7.6-m-high pillars

summarizes the important characteristics of the boundary-element-method model of this mine. Pillar width is 8.5 m, and room width is 9.7 m. Two different pillar models are used, one for 12.1-m-high pillars in the central portion of the mine and the other for 7.6-m-high pillars around the perimeter. Figure 59.28 shows the stress-strain curves for these two pillars with *W/H* ratios of 1.17 and 0.70 respectively.

In the two-step model, the applied vertical stress of 7.5 MPa loads most of the pillars to about 37.5 MPa giving them a safety strength factor of about 1.06. In the second mining step, failure of a third pillar in the array leads to collapse throughout the entire area. As shown in Figure 59.27, the actual failure stopped far short of that predicted by these simplistic numerical model calculations, which may imply considerable conservatism in the models.

Figures 59.29 and 59.30 show the stress and convergence before and after the failure. Stresses decrease from values near the peak stress to residual values while convergence increases dramatically. As in the previous unstable simulations, a small disturbance or increment of mining triggers a very large increment of failure in the model.

From the stress-strain curves input to the model, postfailure stiffness K_P is −240,000 MN/m. Local mine stiffness (K_{LMS}) calculated at central pillars in the array ranges from −200,000 MN/m

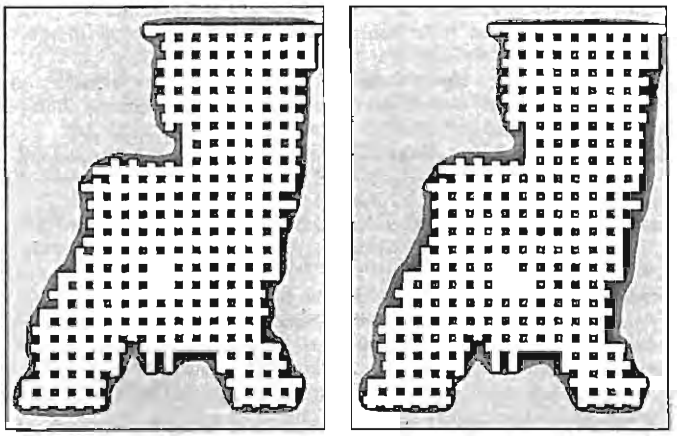

FIGURE 59.29 Metal mine stress before and after CPF. Light to dark gray indicates increasing vertical stress magnitude.

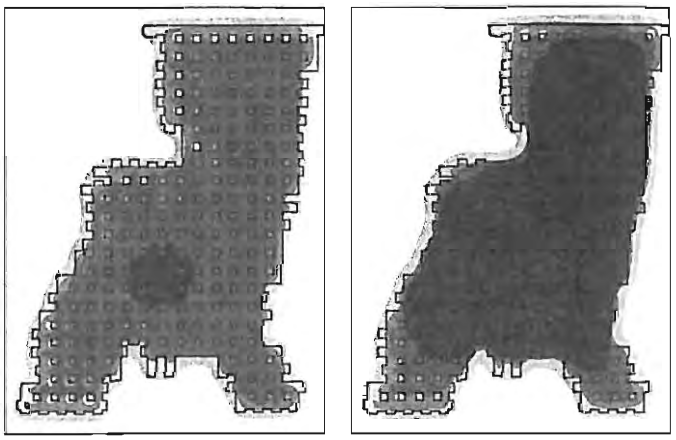

FIGURE 59.30 Metal mine convergence before and after CPF. Light to dark gray indicates increasing convergence stress magnitude.

prior to failure to as low as −27,800 MN/m at the moment of failure. Therefore, unstable failure is always possible by the criterion. As in previous examples, the K_{LMS} value calculated during the failure process is much less in magnitude than values calculated well before or well after failure. Unfortunately, very little is known of the postfailure behavior of mine pillars; however, calculations of K_{LMS} from collapse case histories can provide bounding estimates for K_P.

59.8 SUMMARY AND CONCLUSIONS

Catastrophic collapse or cascading pillar failure (CPF) is a potential problem faced by all room-and-pillar mining operations. CPF occurs when one pillar fails suddenly, which then overstresses the neighboring pillars causing them to fail, and so forth, in very rapid succession. Within seconds, very large mining areas can collapse via this mechanism while giving little or no warning. The collapse itself poses grave danger to miners. In addition, the collapse can induce a violent air blast that disrupts or destroys the ventilation system. Further grave danger to miners exists if the mine atmosphere becomes explosive as a result of CPF.

This paper has documented over 21 collapses that have occurred in the past 20 years mainly in U.S. room-and-pillar mines. Most of these collapses happened in coal mines since substantial production tonnage still comes from room-and-pillar mines; however, huge collapses have also occurred in various metal mines (lead and copper) as well as nonmetal mines (trona, salt, and limestone). Many other similar collapses are known to have occurred around the world. CPF, also known as massive pillar collapse, domino-type failure, or progressive pillar collapse, is the likely mechanism underlying these mine failures. The three case histories given in the paper (Figures 59.17, 59.20 and 59.27) show that the risk of CPF is most acute where large arrays of developed pillars exist without interruption by substantial barrier pillars.

Traditional strength-based design methods are not sufficient to eliminate the possibility of CPF in room-and-pillar mines, and the number of documented collapses in the United States alone provides mute testimony to that statement. Pillar arrays with large average strength safety factors can fail in a domino-type failure (CPF) if just a few pillars in the array begin to fail. Pillars with large strength-based safety factors (for example 1.5) still have a finite probability of failure, and if the number of pillars in an array is large, failure somewhere in the array can become a near certainty, and that failure could in turn initiate CPF.

Traditional strength-based design begins by estimating pillar stress using tributary area method, boundary-element-methods or other numerical methods. Next, various empirical pillar strength formulas or rock mass failure criteria such as the Hoek-Brown criterion provide estimates of the peak pillar strength. Finally, a strength-based safety factor is computed as strength over stress. The traditional approach provides required panel pillar size and barrier pillar size for room and pillar layout; however, this approach does not provide panel pillar width nor does it give any consideration to what might happen if pillars somewhere in the array begin to fail. More advanced rock mechanics considerations such as the local mine stiffness stability criterion provide this design information and a rational basis to eliminate domino-type pillar failures or CPF.

The mechanics of CPF are well understood. Strain-softening behavior is the essential mechanical characteristic of pillars that fail rapidly via this mechanism. Pillars that exhibit strain-softening behavior undergo a rapid decrease in load-bearing capacity upon reaching their ultimate strength. The strain-softening behavior of pillars depends on both inherent material properties and geometry. Pillars with low W/H ratio exhibit a greater degree of strain-softening behavior than pillars with a higher W/H ratio, which typically have elastic-plastic or strain-hardening material behavior.

The local mine stiffness stability criterion developed by Salamon (1970) provides a means to distinguish between mine layouts that fail in a stable nonviolent manner and those that fail in an unstable violent manner via CPF. Simple quasi-three-dimensional boundary-element-method programs such as MULSIM/NL or LAMODEL with strain-softening material models can calculate local mine stiffness (K_{LMS}) and evaluate the stability criterion. These computer programs apply to a wide variety of thin, tabular, bedded-type deposits amenable to room-and-pillar mining methods.

Field data on the complete stress-strain behavior of full-scale mine pillars is limited. The best data is for coal (Zipf 1999). Nevertheless, enough is known to evaluate the stability criterion and assess various mine layouts for their potential to fail via CPF. Three case studies of CPF are examined, and all three probably violated the local mine stiffness stability criterion.

Three stability-criterion-based design approaches are suggested to minimize the risk of CPF, namely, containment, prevention, and full extraction. If an array of pillars violates the local mine stiffness stability criterion, the containment approach applies as shown in Figure 59.11. Low W/H ratio panel pillars that violate the stability criterion are surrounded by high W/H ratio barrier pillars that shield the panel pillars from full tributary area stresses and "contain" panel pillar failure should it initiate. However, if all the panel pillars in an array satisfy the stability criterion, then the prevention approach applies. The panel pillars

do not exhibit much strain-softening behavior because their *W/H* ratio is sufficiently high (probably greater than 3 or 4). In the full extraction approach, the stability issue becomes a moot point, because complete and controlled opening closure occurs immediately after the completion of retreat mining.

Large mine collapses can pose enormous safety hazards to miners and room-and-pillar mining operations. Mining engineers can limit the danger of CPF through prudent application of the local mine stiffness stability criterion and the three stability-criterion-based design approaches suggested to decrease the risk of CPF.

59.9 REFERENCES

Abel, J.F. (1988). Soft Rock Pillars. *Int. J. Min. & Geol. Eng.*, Vol. 6, pp. 215–248.

Aggregate Handbook. (1991). National Stone Association, Washington, D.C.

Bieniawski, Z.T. (1967). The Mechanism of Brittle Fracture of Rock. *Int. J. of Rock Mech. and Min. Sci.* Vol. 4, pp. 396–435.

Bieniawski, Z.T. (1968a). The Effect of Specimen Size on Compressive Strength of Coal. *Int. J. of Rock Mech. and Min. Sci.* Vol. 5, pp. 325–335.

Bieniawski, Z.T. (1968b). In Situ Strength and Deformation Characteristics of Coal. *Engng. Geol.* Vol. 2. pp. 325–340.

Bieniawski, Z.T. (1992). Ground Control. *SME Mining Engineering Handbook*, 2nd Edition, H.L. Hartman, Ed., Society for Mining, Metallurgy, and Exploration, Inc., Littleton, CO, pp. 897–937.

Brady, B.H.G. and E.T. Brown. (1993). Rock Mechanics for Underground Mining. Kluwer Academic Publishers, Boston, 571 pp.

Bryan, A., J.G. Bryan, and J. Fouche. (1966). Some Problems of Strata Control and Support in Pillar Workings. *The Mining Engineer*, Vol. 123, pp. 238–254.

Bullock, R.L. (1982). General Mine Planning. *Underground Mining Methods Handbook*, W.A. Hustrulid, ed., SME of AIME, New York, pp. 113–137.

Bunting, D. (1911). Chamber Pillars in Deep Anthracite Mines. *Transactions*, AIME, Vol. 42, pp. 235–245.

Chase, F.E., R.K. Zipf, and C. Mark. (1994). The Massive Collapse of Coal Pillars–Case Histories from the United States. *Proc. 13th Int. Conf. on Ground Control in Mining*, West Virginia University, Morgantown, WV, pp. 69–80.

Chase, F.E. et al. (1996). Practical Aspects of Mobile Roof Support Usage. *Proc. 15th Int. Conf. Ground Control in Mining*. Golden, CO: Colorado School of Mines.

Coal Data 1999 Edition, National Mining Association, Washington, D.C.

Coates, D.F. (1981). Rock Mechanics Principles. CANMET Monograph 874, Ottawa, Canada.

Cook, N.G.W. and J.P.M. Hojem. (1966). A Rigid 50-Ton Compression and Tension Testing Machine. *J. S. Afr. Inst. Mech. Engr.* Vol. 1, pp. 89–92.

Das, M.N. (1986). Influence of Width/Height Ratio on Postfailure Behavior of Coal. *Int. J. of Mining and Geological Engineering*. Vol. 4, pp. 79–87.

Davidson, J. (1987). Ground Stability Evaluation–Troy Mine–ID No. 24-01467. Mine Safety and Health Administration, Denver, CO. 15 pp.

Denk, J.M., J.J. Jansky, M.T. Hoch, G.J. Karabin, and D.T. Kirkwood. (1994). Accident Investigation Report–Akzo Nobel Salt, Inc. ID. No. 30-00662. Mine Safety and Health Administration, Pittsburgh, PA. 141 pp.

Dismuke, S.R., W.W. Forsyth, and S.B.V Stewart. (1994). The Evolution of Mining Strategy Following the Collapse of the Window Area at the Magmont Mine, Missouri. *Proceedings of District 6 CIM Annual General Meeting*. Metal Mining, pp. 3–8.

Dravo Corp. (1974). Analysis of Large Scale Non-coal Underground Mines. U.S. Bureau of Mines Contract Report SO 122-059, 605 pp.

Examine^{TAB}. 2000. Rocscience Inc., Toronto, Canada, (http://www.rockscience.com).

Farmer, I.W. (1985). Coal Mine Structures. Chapman and Hall, London, 310 pp.

Farmer, I.W. (1992). Room and Pillar Mining. *SME Mining Engineering Handbook*, 2nd Edition, H.L. Hartman, Ed., Society for Mining, Metallurgy, and Exploration, Inc., Littleton, CO, pp. 1681–1701.

Galvin, J. (1992). A Review of Coal Pillar Design in Australia. *Proc. of the Workshop on Coal Pillar Mechanics and Design*, U.S. Bureau of Mines IC 9315, pp. 196–213.

Greenwald, H.P., H.C. Howarth and I. Hartman. (1939). Experiments on the Strength of Small Pillars of Coal. U.S. Bureau of Mines, Technical Paper 605.

Hardy, M.P. and J.F.T Agapito (1977). Pillar Design in Underground Oil Shale Mines. *Proceedings 16th U.S. Rock Mechanics Symposium*, University of Minnesota, Minneapolis, MN, pp. 257–266.

Heasley, K.A. (1997). A New Laminated Overburden Model for Coal Mine Design. *Proceedings: New Technology for Ground Control in Retreat Mining*, NIOSH IC 9446, pp. 60–73.

Heasley, K.A. (1998). Numerical Modeling of Coal Mines with a Laminated Displacement-Discontinuity Code. Ph.D. Dissertation, Colorado School of Mines, 187 pp.

Hoek, E. and E.T. Brown. (1980). Underground Excavations in Rock. Institution of Mining and Metallurgy, London, 527 pp.

Hoek, E., P.K. Kaiser and W.F. Bawden (1995). Support of Underground Excavations in Hard Rock. A.A. Balkema, Rotterdam, 215 pp.

Holland, C.T. (1964). Strength of Coal in Mine Pillars. *Proceedings 6th U.S. Symposium on Rock Mechanics*, University of Missouri, Rolla, pp. 450–466.

Itasca. (1995). FLAC–Fast Lagrangian Analysis of Continua–Version 3.3–User's Manual. Itasca Consulting Group, Inc., Minneapolis, MN.

Jaeger, J.C. and N.G.W. Cook. (1979). Fundamentals of Rock Mechanics. Chapman and Hall, 3rd. ed. 593 pp.

Khair, A.W. and S.S. Peng (1985). Causes and Mechanisms of Massive Pillar Failure in a Southern West Virginia Coal Mine. *Mining Engineering*, Vol. 37, No. 4, pp. 323–328.

Knoll, P. (1990). The Fluid-Induced Tectonic Rockburst of March 13, 1989 in the "Werra" Potash Mining District of the GDR (First Results). *GerL Beitr. Geophysik–Leipzig*, Vol. 99, No. 3, pp. 239–245.

Koehler, J.R. and S.C. Tadolini. (1995). Practical Design Methods for Barrier Pillars. U.S. Bureau of Mines IC 9427, 19 pp.

Mark, C. and A.T. Iannacchione. (1992). Coal Pillar Mechanics: Theoretical Models and Field Measurements Compared. *Proc. of the Workshop on Coal Pillar Mechanics and Design*, U.S. Bureau of Mines IC 9315, pp. 78–93.

Mark C., F.E. Chase, and A.A. Campoli. (1995). Analysis of Retreat Mining Pillar Stability. *Proc. 14th Conf. Ground Control in Mining*, West Virginia University, pp. 63–71.

Mark, C. and F.E Chase. (1997). Analysis of Retreat Mining Pillar Stability (ARMPS). *Proceedings: New Technology for Ground Control in Retreat Mining*, NIOSH IC 9446, pp. 17–34.

Mark, C. and T.M. Barton (1997). Pillar Design and Coal Strength. *Proceedings: New Technology for Ground Control in Retreat Mining*, NIOSH IC 9446, pp. 17–34.

Mark, C. (1999). Empirical Methods for Coal Pillar Design. *Proceedings of the Second International Workshop on Coal Pillar Mechanics and Design*, NIOSH IC 9448, pp. 145–154.

Mine Safety and Health Administration, 1996. "Report of Technical Investigation, Underground Non-metal Mine, Mine Collapse Accident", Solvay Mine, Solvay Minerals Inc., Green River, Sweetwater County, Wyoming, February 3, 1995.

Mokgokong, P.S. and S.S. Peng (1991). Investigation of Pillar Failure in the Emaswati Coal Mine, Swaziland. *Mining Sci. and Tech.* Vol. 12, pp. 113–125.

Obert, L. and W.I. Duvall, (1967). Rock Mechanics and the Design of Structures in Rock. Wiley, New York, 650 pp.

Richmond, R. (1998). Report of Investigation (Underground Coal Mine), Nonfatal Roof-Fall Accident, Red Oak Mine, ID. No. 46-08135, Mine Safety and Health Administration, District 4, Mount Hope, West Virginia.

Ropchan, D. (1991). Ground Support Evaluation–Belinda No. 2 Mine–ID No. 42-01280. Mine Safety and Health Administration, Denver, CO. 12 pp.

Salamon, M.D.G. and A.H. Munro. (1967). A Study of the Strength of Coal Pillars. *Journal of the South African Institution of Mining and Metallurgy*, Vol. 68, pp. 55–67.

Salamon, M.D.G. (1970). Stability, Instability, and Design of Pillar Workings. *Int. J. of Rock Mech. and Min. Sci.* Vol. 7, pp. 613–631.

Sheorey, P.R., D. Barat, K.P. Mukherjee, R.K. Prasad, M.N. Das, G. Banerjee and K.K. Das (1995). Application of the Yield Pillar Technique for Successful Depillaring Under Stiff Strata. *Int. J. of Rock Mech. and Min. Sci. & Geomech. Abstr.* Vol. 32, No. 7, pp. 699–708.

Skelly, W. A., J. Wolgamott, and F. D. Wang. (1977). Coal Pillar Strength and Deformation Prediction Through Laboratory Sample Testing. *Proc. 18th U.S. Rock Mechanics Symposium*, Col. Sch. Mines, Golden, CO, pp. 2B5-1 to 2B5-5.

Spruell, J.L. (1992). Accident Investigation Report–Unimin Specialty Minerals, Inc. Birk 2A–ID No. 11-02598. Mine Safety and Health Administration, Duluth, MN. 12 pp.

Straskraba V. and J.F. Abel (1994). The Differences in Underground Mines Dewatering with the Application of Caving or Backfilling Mining Methods. *Mine Water and the Environment*, Vol. 13, No. 2, pp. 1–20.

Swanson, P.L. and F. Boler (1995). The Magnitude 5.3 Seismic Event and Collapse of the Solvay Trona Mine: Analysis of Pillar/Floor Failure Stability. U.S. Bureau of Mines OFR 86-95, 82 pp.

Touseull J. and C. Rich (1980). Documentation and Analysis of a Massive Rock Failure at the Bautsch Mine, Galena, Ill. U.S. Bureau of Mines RI 8453, 49 pp.

USGS Mineral Industry Surveys. (1998). U.S. Geological Survey, Reston, VA.

Van Heerden, W.L. (1975). In Situ Determination of Complete Stress-Strain Characteristics of Large Coal Specimens. *J. S. Afr. Inst. Min. and Metall.*, Vol. 75, No. 8, pp. 207–217.

Wagner, H. (1974). Determination of the Complete Load-Deformation Characteristics of Coal Pillars. *Proc. of 3rd Int. Congress on Rock Mechanics*, Natl. Acad. Sci. Vol. 2B, pp. 1076–1081.

Wawersik, W.R. and C. Fairhurst (1970). Study of Brittle Rock Fracture in Laboratory Compression Experiments. *Int. J. Rock Mech. and Min. Sci.* Vol. 7, pp. 561–575.

Zipf, R.K. (1992a). *MULSIM/NL Theoretical and Programmer's Manual.* U.S. Bureau of Mines IC 9321, 52 pp.

Zipf, R.K. (1992b). *MULSIM/NL Application and Practitioner's Manual.* U.S. Bureau of Mines IC 9321, 48 pp.

Zipf, R.K. (1996). Analysis and Design Methods to Control Cascading Pillar Failure in Room-and-Pillar Mines. *Milestones in Rock Engineering*, Z.T. Bieniawski ed. Rotterdam: Balkema, pp. 225–264.

Zipf, R.K. (1999). Catastrophic Collapse of Highwall Web Pillars and Preventative Design Methods. *Proc. 18th Int. Conf. on Ground Control in Mining*, West Virginia University, Morgantown, WV, pp. 18–28.

Zipf, R.K. and P.L. Swanson. (1999). Description of a Large Catastrophic Failure in a Southwestern Wyoming Trona Mine. *Proc. 37th U.S. Rock Mechanics Symposium*, Vail, CO, pp. 293–298.

UNDERGROUND
Mining Methods

Engineering Fundamentals and International Case Studies

Edited by William A. Hustrulid and Richard L. Bullock

Published by the
Society for Mining, Metallurgy, and Exploration, Inc.

Society for Mining, Metallurgy, and Exploration, Inc. (SME)
8307 Shaffer Parkway
Littleton, Colorado, USA 80127
(303) 973-9550 / (800) 763-3132
www.smenet.org

SME advances the worldwide minerals community through information exchange and professional development. SME is the world's largest professional association of minerals professionals.

Disclaimer
The papers contained in this volume are published as supplied by individual authors. Any statement or views presented here are those of individual authors and are not necessarily those of the Society for Mining, Metallurgy, and Exploration, Inc. The mention of trade names for commercial products does not imply the approval or endorsement of SME.

Cover images contributed by The Itasca Consulting Group, the Climax Molybdenum Company, and LKAB.

ISBN 0-87335-193-2

Library of Congress Cataloging-in-Publication Data

Underground mining methods : engineering fundamentals and international case studies /
edited by William A. Hustrulid and Richard L. Bullock.
p. cm.
Includes bibliographical references and index.
ISBN 0-87335-193-2
1. Mining engineering. I. Hustrulid, W.A. II., Bullock, Richard L.

TN145.U53 2001
622.2--dc21 2001027301